Publisher version: https://doi.org/10.1016/j.ssi.2022.115858

Graphene oxide-naphthalene sulfonate blends as possible proton exchange membranes

Matteo Di Virgilio[a], Andrea Basso Peressut[a,*], Saverio Latorrata[a],
Marco Mariani[b] and Giovanni Dotelli[a]

[a]Politecnico di Milano, Department of Chemistry, Materials and Chemical Engineering "Giulio Natta",
Piazza Leonardo da Vinci 32, 20133 Milano, Italy
[b]Politecnico di Milano, Department of Mechanical Engineering,
Via La Masa 1, 20156 Milano, Italy

e-mail addresses: matteo.divirgilio@polimi.it
andreastefano.basso@polimi.it
saverio.latorrata@polimi.it
marco.mariani@polimi.it
giovanni.dotelli@polimi.it

[*]Corresponding author: Andrea Basso Peressut
e-mail address: andreastefano.basso@polimi.it
Phone: (IT) +39 02 2399 3190

Publisher version: https://doi.org/10.1016/j.ssi.2022.115858

Abstract

This work presents a study on the preparation of novel self-assembling naphthalene sulfonate-functionalised graphene oxide membranes, whose analysis aims at assessing their potentiality as an alternative to perfluorinated proton conductors. Three different graphene oxide-to-naphthalene sulfonate molar ratios and two different process temperatures were combined to identify the most suitable conditions to perform an effective functionalisation. ATR-FTIR, Raman and EDX spectroscopies, thermogravimetric analysis, static contact angle evaluation and XRD aimed to point out the introduction of sulfonic acid groups ($–SO_3H$) in the GO framework, while optical and scanning electron microscopies verified the good membrane uniformity. The evaluation of the ion exchange capacity (IEC) demonstrated the proton-exchanging ability of the prepared membranes. The most promising sample underwent water uptake (WU) and electrochemical impedance spectroscopy (EIS) tests to examine the dependence of its water sorption and proton conductivity with respect to relative humidity and temperature, in order to deepen the assessment of its feasibility as a possible future electrolyte in alternative energy generators. A preliminary investigation of the mechanical properties of the above-mentioned sample was performed as well to expand the characterisation of its behaviour.

Keywords: graphene oxide; naphthalene sulfonate; proton exchange membrane; materials characterisation; proton conductivity

Publisher version: https://doi.org/10.1016/j.ssi.2022.115858

1. Introduction

The current energy system is becoming more and more unsustainable. Global energy demand is projected to grow at a 1 per cent a year-rate, up to about 230000 TWh by 2050 [1], pushed by the parallel rise of world population at the same pace, up to 9.7 billion people in the next three decades [2,3]. Fossil fuels still cover about 79% of the primary energy consumption, but sources' depletion and the greater awareness of public opinion on environmental themes is compelling the scientific community to turn attention on renewable energy.

Fuel cells and, in particular, Proton Exchange Membrane Fuel Cells (PEMFCs), are deservedly gaining consideration as one of the most promising alternative energy sources, due to a higher efficiency than conventional heat engines and theoretically no emissions. Moreover, their compact designs, absence of moving parts and low temperatures of operation make them ideal power sources for both stationary and automotive applications. Even though the commercialisation has already begun, their competitiveness will be attained only through the optimisation of components, performances (output power densities > 1 W cm^{-2}) and durability (8000–80000 hours) [4–6].

The core of a PEMFC is the proton exchange membrane and Chemours Nafion® is at present the most widespread electrolyte. Nafion® is a perfluorosulfonate copolymer whose lateral hydrophilic sulfonic acid groups (–SO_3H) ensure a proton conductivity higher than 0.1 S cm^{-1} in appropriate levels of humidification conditions [7,8]. Furthermore, it features a reduced permeability to gases and suitable thermo-mechanical properties, albeit some disadvantages limit its performances: it can operate only in a restricted temperature range (60–80 °C) to avoid dehydration and a subsequent drastic conductivity drop; it is rather expensive (about 0.25 € cm^{-2}); it is subjected to a deterioration in structural stability when its glass transition temperature (≈ 110 °C) is approached [9]; it is more prone to fuel crossover at lower thicknesses [7].

Therefore, the detailed study of novel materials able to replace Nafion® is recently occupying most of the research in this field [10–18]. Potential candidates should perform better than Nafion® in conditions of higher temperature and low relative humidity (RH), whose benefits range from the promotion of a faster and more efficient kinetics to the simplification both in water management and cell design. Moreover, they should ensure low electron conductivity, negligible hydrogen and oxygen permeability, chemical, thermal and mechanical stability, in order to meet the requirements for an efficient fuel cell operation [19]. Chemical modification of the perfluorinated sulfonic acid (PFSA) structure, fabrication of hybrid Nafion®-based copolymers or evaluation of the feasibility of different sulfonated and non-sulfonated ionomers are some of the primarily investigated solutions to accomplish these complicated goals.

Amongst several examined species, graphene oxide (GO) is earning remarkable appeal due to its noteworthy electronic insulation, self-assembling ability, mechanical properties and large surface area [20–22]. According to various proposed structural models [21], GO is characterised by the simultaneous presence of unoxidized benzene rings and oxygenated functionalities on aliphatic rings both in planar (epoxy, hydroxyl and carbonyl groups) and lateral position (carboxyl and hydroxyl ones). The amphiphilicity associated to the coupling of sp^2- and sp^3-hybridised carbon atoms generates hydrophobic and hydrophilic regions that may help water retention and consequently protons movement [23–25]. Bayer et al. [8] have prepared and analysed a self-standing GO membrane, observing moderately higher water uptake and swelling ratio with respect to Nafion®. While the first result suggested a greater water sorption capacity and thereby a probable higher proton conductivity in low humidity conditions, the second one revealed a detrimental thickness sensitivity to repeated hydration-drying cycles at the membrane-catalyst interface. Furthermore, GO displayed overall better mechanical characteristics than the conventional electrolyte, and an interesting through-plane proton conductivity of 0.55 mS cm^{-1} at 70 °C and 100% RH.

Publisher version: https://doi.org/10.1016/j.ssi.2022.115858

The functionalisation of GO skeleton with acid groups, for example sulfonic ones (–SO_3H) [9,26–30] is considered an attractive approach to conveniently tune the features of this material. Sulfonated graphene oxide (SGO) is a promising candidate for PEMFC applications, as it fuses together GO strengths and an elevated concentration of oxygen-bearing moieties, amongst which sulfonic groups (–SO_3H) provide a resemblance with the pendant chains of sulfonated ionomers. Ravikumar et al. [9] have fabricated and tested self-standing SGO sheets, whose through-plane proton conductivity reached 12 mS cm^{-1} at 30 °C and 100% RH, considerably improving that of unfunctionalized GO.

This work aspires to assess an innovative GO functionalisation method that involves a reaction with naphthalene sulfonate (NS) compounds, which are amongst the most important and readily accessible derivatives of naphthalene [31–33]. They own a strong acid behaviour in solution and an extreme solubility in water. These species should be more compatible with the GO framework by virtue of their bulky aromatic rings that can establish π-π interactions [34], differently from those described in literature, such as sulfanilic [26] and chlorosulfonic acid [27]. Amongst the analysed sulfonating agents, naphthalene sulfonate molecules have proven useful to mitigate dehydration issues at reduced humidity and elevated temperatures. Turley et al. [35,36] have employed them for the functionalisation of the inner pore walls of mesoporous ceramic oxides, in order to foster proton transport in the abovementioned conditions; their composites exhibited promising proton conductivity values, up to about 21 mS cm^{-1} at 100 °C, 50% RH, one order of magnitude better than Nafion® in the same situation. Shudo et al. [34] have exploited the development of π-π stacking interactions to intercalate NS derivatives into GO, producing a hybrid solid electrolyte which displays an improved proton conductivity with respect to the virgin material. Values about 1.8 mS cm^{-1} at 85 °C, 40% RH have been obtained, more than one order of magnitude higher than those of GO in the same environment.

One of the most interesting techniques to fabricate GO-based membranes is layer-by-layer (LBL) self-assembly, which has been increasingly exploited in recent studies due to its merit of overcoming issues of components' dispersion typical of conventional solution casting methods. Jia et al. [37] have developed a LBL self-assembly procedure based on the repeated alternate deposition of polyurethane (PU), GO, poly(diallyldimethylammonium chloride) (PDDA) and again GO on a glass substrate up to the obtainment of a free-standing $(PU/GO/PDDA/GO)_{200}$ membrane. In a comparable manner, Shen et al. [38] have constructed depositional $SPVDF(CS/GO)_{50}$ PEMs starting from a sulfonated poly(vinylidene fluoride) (SPVDF) substrate, onto which chitosan (CS) and GO have been deposited through an alternate dipping.

Differently, a controlled self-assembly of the functionalised GO membranes via vacuum filtration has been chosen for the present work. Such procedure allows an easy manufacture of uniform, well-ordered multilayer sheets with precise thickness by means of a directional flow promoted by vacuum conditions [39]. Three GO-to-NS molar ratios have been investigated to understand the effect of this parameter on the fabrication process. In the same way, the influence of temperature has been studied by adopting two different operating conditions for each molar ratio. The obtained samples have undergone a detailed morphological and microstructural characterisation by means of optical microscopy (OM), attenuated total reflection Fourier-transform infrared (ATR-FTIR), Raman and energy dispersive X-ray (EDX) spectroscopies, thermogravimetric analysis (TGA), scanning electron microscopy (SEM), static optical contact angle (OCA) measurements and X-ray diffraction (XRD) experiments. Additionally, the ion exchange capacity (IEC) has been evaluated to assess the ability of the produced membranes to carry protons. The most promising membrane has been further examined with a preliminary investigation of its water uptake and proton conductivity at several combinations of temperature and relative humidity (RH), as well as of its mechanical properties. A comparison with benchmark samples of pure GO and Nafion® 212, extensively analysed in previous works amongst the authors' research group [40,41], has permitted to demonstrate the appeal of these materials as potential proton conductors to be further investigated for their possible implementation in future electrochemical energy generators.

Publisher version: https://doi.org/10.1016/j.ssi.2022.115858

2. Materials and methods

2.1 Membranes fabrication

The produced membranes have been denominated X-GONS-TY, in which GO stands for graphene oxide, NS indicates naphthalene sulfonate, X represents the GO term in the GO-to-NS molar ratio and TY specifies the final process temperature, as explained in Figure 1.

The methodology adopted for the preparation of the X-GONS-TY membranes has been inherited from a previous work within the authors' research group [40,41], albeit some substantial modifications were necessary. Preliminarily, a naphthalene sulfonate sodium salt aqueous solution (commercial name Flube OS-39, acquired from Bozzetto Group) has been oven-dried at 120 °C for 1 hour to favour the recovery of the NS sodium salt. The residual solid has been accurately grinded in a mortar and the resulting fine powder, properly weighed in a beaker, has been acidified to restore the naphthalene sulfonic acid form by substituting the Na^+ cations with H^+ ions. This procedure has been completed by pouring into the beaker the proper volume of a 2 M nitric acid aqueous solution via an automatic pipette (Transferpette®, BRAND GMBH + CO KG), followed by dilution with 10 mL of deionised water and magnetic stirring for 20 minutes at 500 rpm. Meanwhile, a round-bottomed flask has been filled up by 25 mL of a GO commercial aqueous dispersion (0.4 wt.%, supplied by Graphenea, Inc.), containing 100 mg of GO, and inserted in the LABSONIC LBS 1-H3 (Falc Instruments s.r.l.) for 10 minutes. A mild ultrasonication has been performed in an ice bath to achieve a strong homogenisation while limiting overheating and, consequently, a possible undesired GO thermal reduction. Afterwards, the previously prepared acidified NS has been trickled into the flask containing the GO mixture. Then, the flask has been inserted into an oil bath, attached to a reflux condenser, and positioned on a magnetic stirrer to blend the dispersion at 500 rpm. As depicted in Figure 1, two different process conditions have been investigated during the stirring phase: Condition A, in which the temperature has been kept to 25 °C for 6 hours; Condition B, in which the temperature has been initially set to 25 °C for 3 hours and then increased to 100 °C for the remaining 3 hours. Subsequently, the mixture has been diluted with 150 mL of deionised water (to raise its pH to avoid possible issues to the pumping system) and vacuum filtered on a Büchner funnel through a Durapore® PVDF filter disk (pore size of 0.22 µm, thickness of 125 µm, supplied by Merck Millipore); this procedure allowed to separate the aqueous medium from the GONS layers and to promote their settling and compacting. Eventually, the obtained self-assembled membrane has been oven-dried at 40 °C.

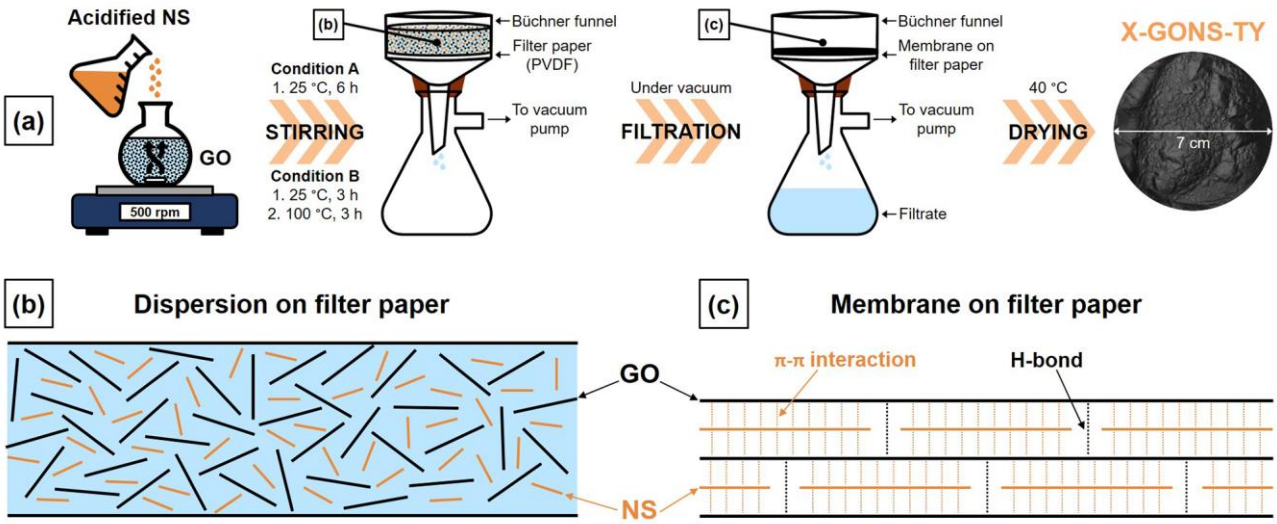

Fig. 1 (a) Scheme of the preparation steps of X-GONS-TY membranes; X identifies the GO-to-NS molar ratio, while TY specifies the final temperature adopted during the stirring phase, i.e., 25 °C in Condition A and 100 °C in

Publisher version: https://doi.org/10.1016/j.ssi.2022.115858

Condition B; (b) details of the dispersion on filter paper during vacuum filtration; (c) details of the membrane on filter paper after vacuum filtration, with established interactions between GO layers and NS groups

2.2 Morphological and microstructural characterisation

Optical microscopy (OM) images have been acquired at 15x magnification with the Olympus trinocular tube SZ4045TR CTV connected to the DFC290 digital CCD camera; their recording and analysis have been performed with the INFINITY ANALYZE software by Lumenera Corporation.

Attenuated total reflection Fourier-transform infrared (ATR-FTIR) spectroscopy has been accomplished on all the as-prepared X-GONS-TY samples by means of a ThermoElectron Continuμm IR microscope coupled with a FTIR Nicolet Nexus spectrometer (Thermo Fisher Scientific). The equipment consisted in a single reflection silicon crystal and a mercury cadmium telluride (MCT) detector cooled by liquid nitrogen. The spectra have been acquired in the wavenumber interval of 650–4000 cm^{-1}, at a resolution of 4 cm^{-1} and with 128 scans.

The Jobin Yvon Labram HR800 Raman spectrometer has been used to perform Raman spectroscopy on the samples, by applying a He-Ne laser (wavelength of 632.8 nm) as exciting source. The laser power has been set to 500 μW through a proper filter, in order to avoid heating effects or laser-induced degradation. The instrument was coupled with the microscope model Olympus BX41 equipped with a 50x objective, under which the samples have been placed to exploit a micro-Raman setup. Spectra have been recorded averaging three acquisitions, each one lasting 30 s.

The EXSTAR 6000 TG/DTA 6300 by Seiko has allowed the execution of thermogravimetric analyses (TGA) on the produced membranes, with the following operating conditions: a heating rate of 10 °C min^{-1} from room temperature to 1000 °C and an inert atmosphere obtained by supplying a 55 mL min^{-1} stream of nitrogen.

Scanning electron microscopy (SEM) images have been acquired by the Cambridge Stereoscan 360 at 500x, 1000x and 5000x magnifications; the chamber pressure has been set to 10^{-5} Pa, while the adopted accelerating voltage and current probe were 20 kV and 200 pA, respectively.

Cross-sectional SEM images at 1000x magnification have been obtained by the Carl Zeiss S.p.A. microscope model EVO 50 EP, as a means of evaluating the thickness of the X-GONS-TY membranes. The same instrument, equipped with the EDX spectrometer model INCA 2000 PENTAFET LZ4 by Oxford Instruments plc, has been employed to perform energy dispersive X-ray (EDX) spectroscopy on the specimens under a variable pressure ranging from 30 to 40 Pa.

Optical contact angle (OCA) measurements have been carried out with the OCA 15 plus, provided by DataPhysics Instruments GmbH, and mounting a 752x582 pixels resolution CCD video-camera able to record up to 50 frames per second. The obtained images were then processed by the software SCA 20.

The diffractometer model D8 Advance by Bruker Corporation has been used for the X-ray diffraction (XRD) analysis. The as-prepared membranes have been irradiated with X-rays characterised by a wavelength of 1.54 Å, emitted by a Cu-Kα filament and filtered through a monochromator. The experiments have been executed at a scanning rate of 0.02° per second in the angular interval of 5–30°, with a count time of 1 s.

2.3 Ion exchange capacity

Ion exchange capacity (IEC) has been determined through a classic acid-base titration technique, specifically following the procedure proposed by Vinothkannan et al. [42]. X-GONS-TY samples have been oven-dried at 60 °C for 1 hour in order to obtain their dry mass, then they have been equilibrated in 250 mL of a 2 M NaCl aqueous solution in order to permit the exchange between H^+ ions and Na^+ ones on the oxygenated and sulfonic acid sites. Eventually, the immersed membrane portions have been withdrawn from the solution, which has been titrated against controlled volumes of a 0.01

M NaOH one. By defining IEC (meq g^{-1}) as the milliequivalents of ionic sites provided with an exchangeable proton per gram of dried species, Equation 1 can be employed to compute it:

$$IEC = \frac{V_{NaOH} \cdot C_{NaOH}}{m_{dry}} \quad (1)$$

V_{NaOH} (mL) is the volume of the NaOH solution extrapolated at the turning point of the titration curve, C_{NaOH} is its concentration (mmol mL^{-1}) and m_{dry} (g) is the pre-equilibration dry mass of the sample.

2.4 Water uptake and swelling ratio

The experimental setup employed for the quantification of water uptake (WU) and swelling ratio (SR) of the most promising X-GONS-TY membrane was comprised of a lab-built humid chamber, a thermohygrometer with external probe model C3121 (Comet System s.r.o.) and a digital micrometer (±1 μm of sensitivity). The dry mass and dry thickness of the samples, cropped in easily manageable rectangular portions, have been measured after 2 hours of oven-drying at 60 °C aimed at evaporating any trace of humidity and excess water trapped in the midst of GO layers. Afterwards, the membrane sections have been introduced in the humid chamber and left for 1 hour to be homogeneously wetted in the desired temperature and relative humidity (RH) settings, with the purpose of understanding how they responded to different operating conditions, reasonably similar to the typical ones of a PEM fuel cell. Five temperatures have been investigated, namely 20, 40, 60, 80 and 100 °C, accurately controlled by an insulated shell with oil recirculation and a thermocouple inserted in the internal environment. The thermohygrometer, characterised by an accuracy of ±2.5% RH in the 5–95% range, was applied to check the level of humidification ensured by 600 mL of deionised water and of a saturated solution of magnesium nitrate hexahydrate ($Mg(NO_3)_2 \cdot 6H_2O$), 95% and 53% RH respectively. These values can be considered adequately constant in the examined temperature interval, as checked in a previous study [43]. Thereafter, the samples have been extracted from the chamber and their surface has been carefully dabbed with paper to remove the excess water drops. Eventually, wet mass and wet thickness were measured, allowing the computation of the corresponding water uptakes and swelling ratios via Equations 2 and 3:

$$WU\ (\%) = \frac{m_{wet} - m_{dry}}{m_{dry}} \cdot 100 \quad (2)$$

$$SR\ (\%) = \frac{t_{wet} - t_{dry}}{t_{dry}} \cdot 100 \quad (3)$$

in which m_{wet} (g) and m_{dry} (g) are the wet and dry masses of the specimens, whereas t_{wet} (μm) and t_{dry} (μm) are the wet and dry thicknesses.

2.5 Proton conductivity

Proton conductivity investigation has relied upon electrochemical impedance spectroscopy (EIS), performed in an experimental apparatus analogous to the one described in Section 2.4. A Teflon® cell has been implemented to hold the sample via clamping between two stainless steel electrodes (Figure S1). Three temperatures (20, 60, 80 °C) and two relative humidities (53, 95%) have been explored to understand their effects on the ionic conductivity, for a total of six different environmental conditions. Conveniently dimensioned samples have been oven-dried at 60 °C for 2 hours; then they have been assembled on the Teflon® holder, inserted in the chamber and exposed to its controlled environment for 1 hour. Afterwards, three measurements have been carried out by means of the Bode Analyser of the STEMlab™ 125-14 board by Red Pitaya. A potentiostatic mode has been adopted by setting a frequency interval of $1–10^7$ Hz and a signal amplitude of 0.5 V. Firstly, the obtained Bode diagrams have been transformed to visualise a Nyquist plot; then, the

software ZView® (Scribner Associates Inc) has been used to fit them. Equation 4 has allowed to infer the proton conductivity σ (S cm^{-1}) as the inverse of the resistivity ρ (Ω cm); the latter has been computed, coherently with the second Ohm's law, as the product of the extracted internal resistance R_i (Ω), the sample's width w (cm) and thickness t (cm) divided by the electrodes inter-distance d (cm), as shown in Figure S1:

$$\sigma = \frac{1}{\rho} = \frac{d}{R_i \cdot w \cdot t} \quad (4)$$

2.6 Mechanical properties

The Synergie 200 test system by MTS Systems Corporation has been used to evaluate the mechanical properties of the most promising X-GONS-TY membrane at room temperature and atmosphere. The test has been conducted on both pristine samples and on specimens previously treated at 80 °C for one hour, in order to assess any temperature effect. Several strips of 70 mm in length, 10 mm in width have been tested in tensile mode by applying a strain rate of 1 mm min^{-1} to measure the corresponding forces and elongations. Tensile strength, strain at break and Young's modulus have been derived as test outputs from the so-obtained stress-strain curves.

The Future Tech FM-810 micro-hardness tester by Kawasaki has been employed to determine the Vickers hardness (VH) of the specimen with the most promising GO-to-NS molar ratio, averaging ten measurements on both virgin and 80 °C-treated samples with an applied load of 300 gf (2.9 N) for 15 s at ambient conditions.

3. Results and discussion

3.1 Membranes fabrication

The key aspect of this work has been the research of an optimised recipe and of the best reaction conditions to attain freestanding ion-conducting membranes with suitable properties for a potential PEMFC application. The innovative production protocol, for which there is a scarcity of established literature references, has been modulated starting from the methodology already discussed in previous works within the authors' group [40,41]. Three different GO-to-NS molar ratios and two different process temperatures have been combined and investigated, for a total of six coherently termed samples (X-GONS-TY, in which X represents the GO content and TY is the final temperature condition). The precise amounts of NS have been calculated on the basis of an estimated GO average molecular mass of 35.3 g mol^{-1} [40,41]. This value is associated to an empirical formula ($C_{1.5}H_{0.2}N_{0.01}S_{0.03}O$), derived from the analysis of the elements contained in the commercial dispersion [44] performed by the supplier. Chemicals and surfactants of the initial mixture, usually added to promote the production of GO and to enhance its in-water dispersibility, are mainly accounted for by the presence of nitrogen and sulphur [20,45]. The carbon-to-oxygen ratio, equal to 1.5, has been computed in a previous work by Basso Peressut et al. [41] as a rounded ratio between the atomic percentages of carbon (55.75%) and oxygen (36.23%). The derivation of the formula has been completed by applying the same calculation to the other elements. EDX spectroscopy compositional results performed on a pure GO membrane have permitted the validation of such formula, since a carbon-to-oxygen atomic percentage ratio of roughly 1.6 has been extrapolated [41]. The proposed formula demonstrates a certain trustworthiness, since it complies with various widely accepted GO structural models reported in literature [21].

Initially, a 1-to-1 molar ratio between the GO substrate and the functionalising agent has been selected as a first try. The 1-GONS-T100 membrane has shown some integrity problems during the separation from the PVDF filter employed in the vacuum filtration step, which have caused its undesired complete fragmentation. This phenomenon may be ascribed to the detrimental effect of the elevated NS content on the overall self-assembling capability of the resulting composite. Consequently, it has been decided to increase the molar ratio to 5-to-1 in order to favour the self-assembling and to attain

Publisher version: https://doi.org/10.1016/j.ssi.2022.115858

a better resemblance to pristine GO in terms of stability and flexibility. As expected, the resulting 5-GONS-T25 and 5-GONS-T100 specimens have demonstrated an improvement in manageability. Lastly, the 10-to-1 molar ratio has been tested to verify if a reduced amount of sulfonating species could still provide a suitable enhancement in the ion exchange propensity while approaching the structural stability typical of bare GO. As a matter of fact, 10-GONS-T25 and 10-GONS-T100 macroscopic appearance was readily comparable to the one of benchmark GO, as visible in Figure 2. Nonetheless, no sensible differences have been detected for the six products from a macro-morphological point of view; this outcome suggests a certain homogeneity in the production method independently from the specific GO-to-NS molar ratio. The chemical compatibility between naphthalene aromatic rings and GO sp^2-hybridised domains could be reckoned as the main reason [46].

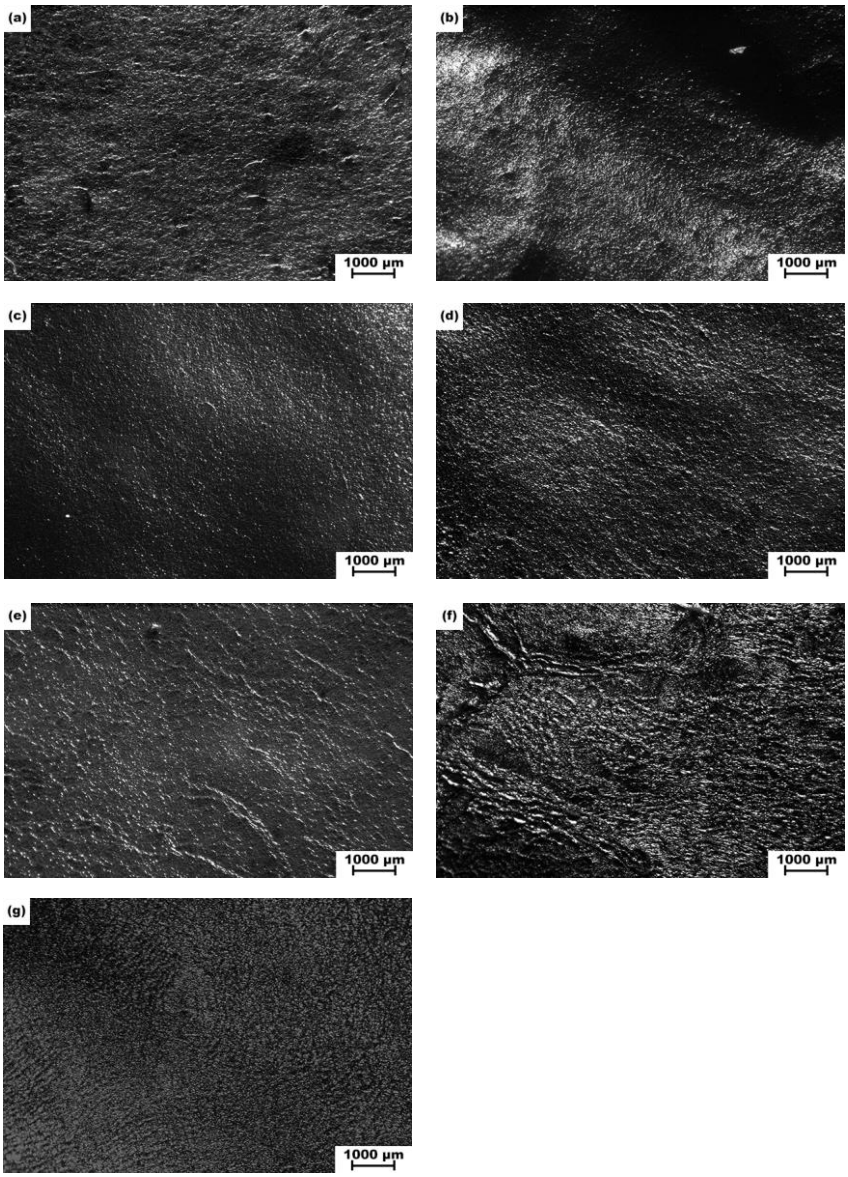

Fig. 2 OM images of the X-GONS-TY samples at 15x magnification: (a) 1-GONS-T25, (b) 1-GONS-T100, (c) 5-GONS-T25, (d) 5-GONS-T100, (e) 10-GONS-T25, (f) 10-GONS-T100, (g) GO reference

Publisher version: https://doi.org/10.1016/j.ssi.2022.115858

3.2 Morphological and microstructural characterisation

3.2.1 Attenuated total reflection Fourier-transform infrared spectroscopy

Attenuated total reflection Fourier-transform infrared (ATR-FTIR) spectra of the synthesised X-GONS-TY membranes are portrayed in Figure 3. This characterisation technique allows to acquire information on the superficial traits of the prepared materials, since the depth of penetration of the evanescent wave emitted in ATR experiments is few micrometres, and it permits to check the effectiveness of the functionalisation via NS compounds from a qualitative standpoint.

X-GONS-TY samples display some contributions that are typical of the GO skeleton, already disclosed in previous works [40,41]. In detail, the bands centred at 981 cm^{-1} and 1032 cm^{-1} might identify the stretching of C–O in unstable lactols and peroxides and C–OH bonds in tertiary alcohols. Besides, the band between 1300 and 1400 cm^{-1} might be assigned to the bending of O–H bonds in hydroxyl, carboxyl, and phenol moieties. Then, the bands centred at 1615, 1730 and 1815 cm^{-1} could be associated to the bending of adsorbed water's O–H bonds, C=O stretching in carboxyl and carbonyl ones and C=O stretching in anhydride groups. Lastly, the structured broad band made of three overlapping contributions located between 3000 and 3600 cm^{-1} can be attributed to O–H stretching in peripheral carboxylic acid moieties, tertiary alcohols, and adsorbed water molecules, respectively.

The successful introduction of NS molecules within the membrane is suggested by the rising of several contributions that hint the presence of species other than GO: the band in the 815–850 cm^{-1} region might be associated to S–OH stretching in $–SO_3H$ groups [47]; the one between 1100 and 1250 cm^{-1} is compatible with the reciprocal in-plane movements of carbon atoms and substituents in the aromatic rings of naphthalene, as well as with the stretching vibrations of O=S=O in sulfonic acid moieties [28,48–50]. Moreover, with respect to pristine GO, a contribution rises in X-GONS-TY membranes at about 1580 cm^{-1}, matching the stretching of C=C bonds in sp^2-hybridised regions. They can be partly ascribed to the aromatic rings of NS molecules, as well as to a broadening of the graphitic domains of GO, potentially caused by a partial reduction of the oxygen-containing sites [42,47]. This observation is strengthened by the lower intensity of the bands attributed to lactols and peroxides (981 cm^{-1}), as if these less stable surface groups are partially removed in X-GONS-TY membranes as a consequence of the sulfonation procedure.

Given the bulky nature of naphthalene sulfonates and the presence of aromatic rings akin to the framework of GO, it is reasonable to expect that the functionalisation does not necessarily involve a chemical reaction with the oxygenated groups of GO. Conversely, as these molecules intercalate within GO flakes there may be the development of preferential π-π interactions amongst NS rings and GO unoxidized domains, favouring the insertion of naphthalene sulfonates within the membrane and an effective functionalisation [34,51]. This hypothesis seems to be supported by comparing from a qualitative point of view the ATR-FTIR spectra of X-GONS-TY specimens in Figure 3a, where it is possible to notice that, even by varying the concentration of the sulfonating agent, the shape of the spectra does not change significantly. Furthermore, the comparison between the spectrum of 5-GONS-T100, taken as an example, and the one of the reference Flube OS-39 NS powder (Figure 3b) shows that most of the original vibrations of the NS molecule do not vary considerably after their insertion in GO, suggesting that only slight chemical modifications take place during the mixing process and become more visible only in the samples prepared at higher process temperatures. In fact, the contributions attributed to NS species seem to be slightly more intense with respect to adjacent bands in the case of T100 membranes, possibly demonstrating a moderate influence of the working temperature on the chemistry of the process, both in terms of potential reduction and of overall effectiveness.

Publisher version: https://doi.org/10.1016/j.ssi.2022.115858

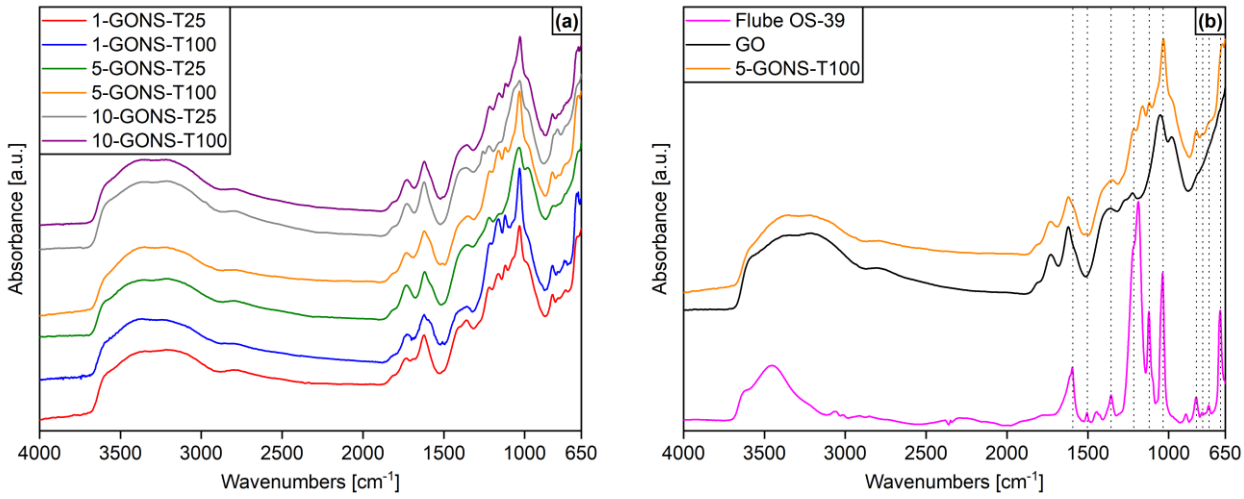

Fig. 3 (a) ATR-FTIR spectra of the investigated X-GONS-TY membranes; (b) comparison amongst the infrared spectra of Flube OS-39 NS powder, GO reference and 5-GONS-T100

3.2.2 Raman spectroscopy

The previous assumptions (Section 3.2.1) seem to be reinforced by the analysis of the Raman spectra of the prepared X-GONS-TY membranes, which are shown in Figure 4, whereas the corresponding bands positions and intensity ratios are summarised in Table 1. Raman spectroscopy allows to investigate the effect of the introduction of NS molecules on the carbonaceous framework of GO, in terms of possible alterations to its characteristic D and G bands. The G band can be related to the presence of graphitic domains, with a typical position of about 1580 cm^{-1} in crystalline graphite [52,53]. Pristine GO displays a slightly blue-shifted G band, centred at about 1601 cm^{-1}, as a consequence of the increase in the number of defects following the oxidation of graphite; this causes the rising of the well-known D (about 1340 cm^{-1}) and D' (about 1620 cm^{-1} and merged with the G band) modes as well [8,54]. In general, the D band becomes more intense as sp^2 hybridisation is interrupted by sp^3 regions involving bonds among carbon atoms and oxygenated functionalities, and the D/G intensity ratio can provide an insight on the proportion between defective and graphitic regions in GO-based specimens [8,52–54]. By comparing the GO reference with X-GONS-TY membranes, it is possible to notice that the Raman spectra of the latter do not vary significantly with respect to those of the virgin material, as suggested by the similar D and G modes positions and intensity ratios. The absence of visible discrepancies appears in agreement with the hypothesis that the introduction of NS species takes place as an intercalation among GO layers, therefore only slightly affecting the original graphitic structure of pristine GO. Non-covalent π-π bonds are likely to be established between the aromatic rings of NS and the sp^2-hybridised regions of GO layers. The chemical compatibility of the involved species has allowed a fostered self-assembling of adjacent GO sheets from the aqueous dispersion up to the formation of stable supramolecular structures. The prepared membranes have disclosed a satisfactory manageability, except for 1-GONS-T100 which appeared more fragile. In the case of high NS content, the steric hindrance of such molecules could have interfered with the generation of non-polar interactions, worsening the overall stability of the sample [34,51].

Publisher version: https://doi.org/10.1016/j.ssi.2022.115858

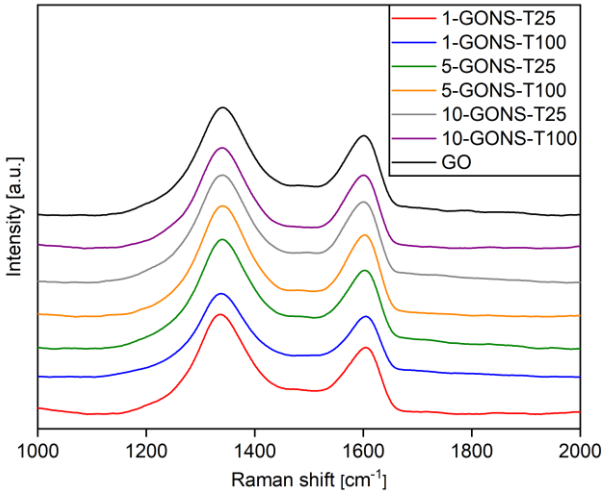

Fig. 4 Raman spectra of the investigated X-GONS-TY membranes and of GO as reference

Table 1. Raman bands positions and intensity ratios of X-GONS-TY membranes and of GO as reference.

Sample	D band position [cm^{-1}]	G band position [cm^{-1}]	D/G intensity ratio
1-GONS-T25	1338	1605	1.50 ± 0.07
1-GONS-T100	1340	1603	1.35 ± 0.03
5-GONS-T25	1341	1602	1.37 ± 0.10
5-GONS-T100	1342	1603	1.35 ± 0.05
10-GONS-T25	1341	1600	1.32 ± 0.01
10-GONS-T100	1341	1601	1.35 ± 0.06
GO	1342	1601	1.43 ± 0.03

3.2.3 Thermogravimetric analysis

The thermograms of the prepared X-GONS-TY samples are illustrated in Figure 5. They have been useful to identify changes in the thermal behaviour of the examined materials and to witness the emissions of oxygenated or sulfonated derivatives, probably symptomatic of the presence of $–SO_3H$ groups.

Four ranges of mass losses can be recognised. The first one, with an average value of 15%, takes place below 110 °C; it is caused by the evaporation of physically adsorbed water, trapped in the GO sheets by the hydrophilic groups. The second one of about 20–35% occurs in the range 175–225 °C and it is associated to the decomposition of oxygenated functionalities (such as epoxides, tertiary alcohols and carboxylic acids) and to the release of CO_x gases [55]. The third one is the smallest (2–5%) and it may be glimpsed between 280 and 300 °C. It can be ascribed to the decomposition of sulfonated moieties covalently bonded to NS compounds intercalated within GO flakes, as witnessed in ATR-FTIR spectra [27,56]. It can be intended as a qualitative proof of the reaction effectiveness, seeing as it is absent in typical GO thermograms (Figure S2a) already discussed in a previous work amongst the authors' research group [41]; however, its limited value could mean a small quantity of inserted S-bearing groups. One can notice that the temperature range at which the desulfonation is triggered in X-GONS-TY samples is less broad than the one of Nafion® 212 (280–380 °C [41]), as visible in Figure S2b. A possible explanation could be the minor stability of the introduced functionalities. A continuous mass loss starts when the experimental temperature overcomes 400 °C. It is included between 20 and 25% and it is linked to the breakdown and partial pyrolysis of the GO stacking due to the weakening of the inter-layer

interactions and to the collapse of the basal plane [20,28,42]. 5-GONS-T100 appears to be the most thermally resistant amongst the synthesised species, especially in the range of operating temperatures of PEMFCs. In fact, it exhibits the smallest adsorbed water mass drop (≈ 10%), suggesting a probable better water retention ability, in agreement with the findings of Shudo et al. [34]. Moreover, it has the positive aspect of a larger residual mass (≈ 40%) with respect to virgin GO (≈ 25% [41]), which could recommend a positive influence of the functionalisation process by means of a reinforcement of the aromatic domains promoted by the interaction with naphthenic fractions.

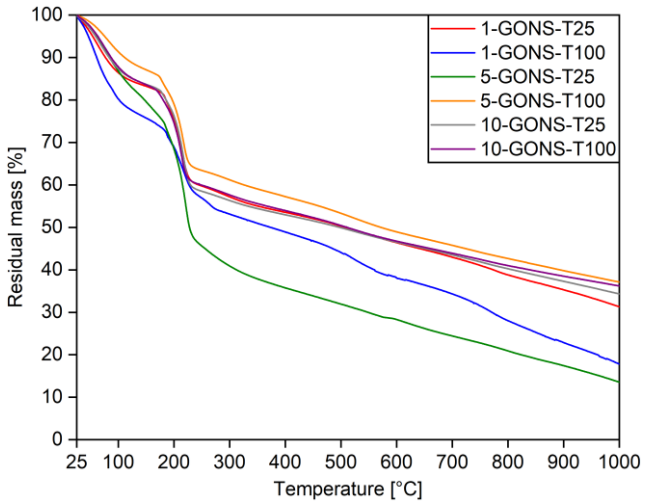

Fig. 5 Thermograms of the investigated X-GONS-TY membranes

3.2.4 Scanning electron microscopy

Scanning electron microscopy (SEM) ensures a complete overview on the morphology of the X-GONS-TY samples at different dimensional scales. Images at 500x, 1000x and 5000x magnifications are collected in Figure 6. They show a relative uniformity and an overall compactness of the structure at the microscopic level. This suggests a decent integration of the functionalising species within the GO matrix and consequentially a possible chemical compatibility between the aromatic portion of the NS molecules and the sp^2-hybridised regions of GO. Surface defectiveness is a common feature of the six samples, mainly as disorder in the flakes packing. 10-GONS-T25 and 10-GONS-T100 display some jagged zones and the highest unevenness, rather similar to that of pristine GO (Figure S3) [41]. This feature is reasonable, since they have been manufactured by employing the largest GO-to-NS molar ratio.

Publisher version: https://doi.org/10.1016/j.ssi.2022.115858

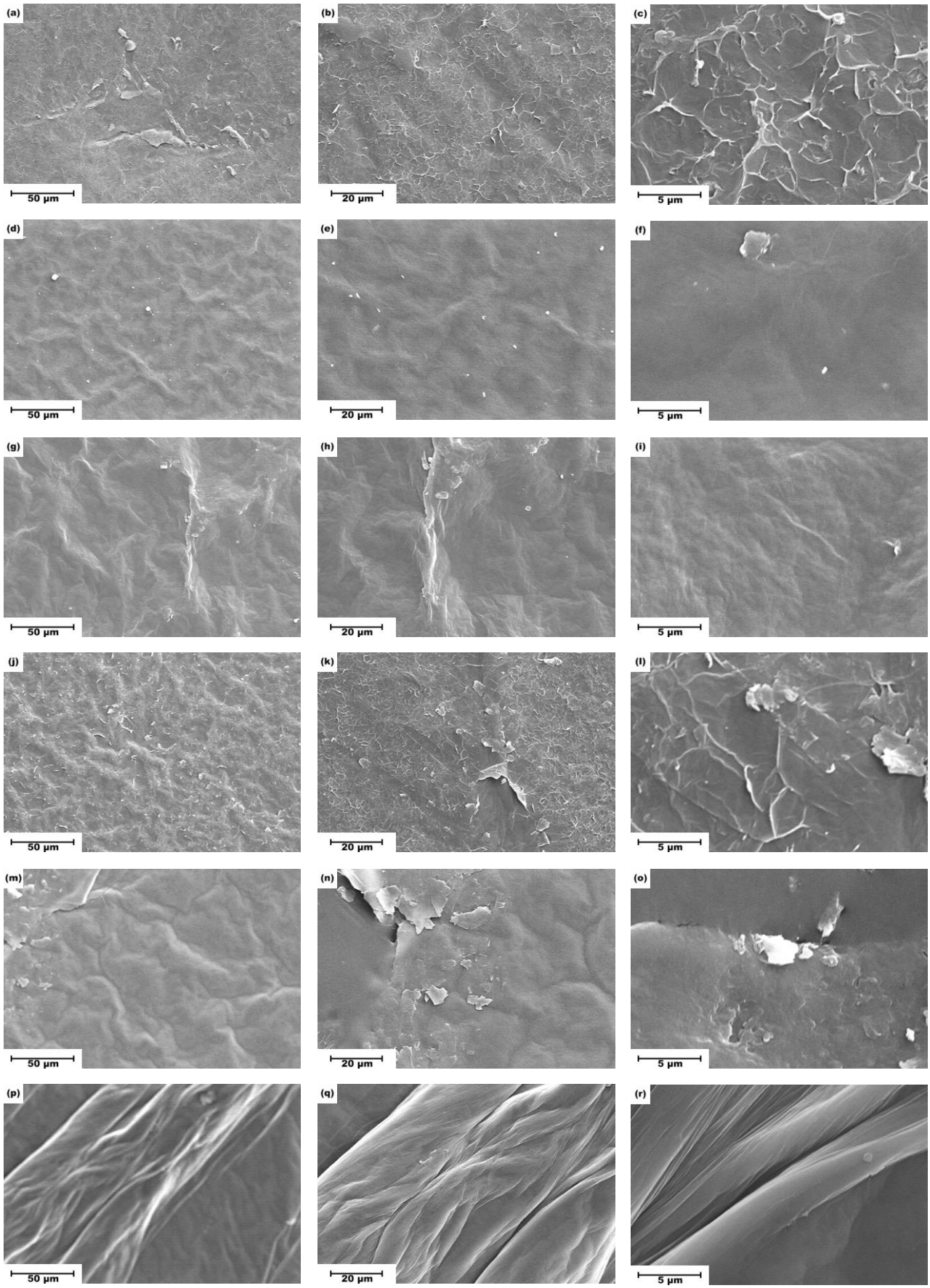

425 **Fig. 6** SEM images of the X-GONS-TY samples at 500x, 1000x and 5000x magnification (from left to right): (a-c) 1-
426 GONS-T25, (d-f) 1-GONS-T100, (g-i) 5-GONS-T25, (j-l) 5-GONS-T100, (m-o) 10-GONS-T25, (p-r) 10-GONS-T100
427

Publisher version: https://doi.org/10.1016/j.ssi.2022.115858

Cross-sectional SEM images at 1000x magnification of the X-GONS-TY samples are displayed in Figure 7, along with a 10000x-magnified image of a reference GO membrane. They have been exploited also for the estimation of the average specimens' thicknesses, which are listed in Table 2. The compactness of the stratified layers in the functionalised samples is comparable to virgin GO (Figure 7g), as already supposed from the surface homogeneity observed in Figure 6. Nevertheless, the thicknesses of the investigated samples differ from the one of GO depending on the employed GO-to-NS molar ratio. 10-GONS membranes, which are prepared with the highest GO content, prove thicknesses between 7.6±0.2 and 9.7±0.3 μm, the closest to their pure precursor (3.6±0.2 μm). Values coherently increase up to 17.3±1.1 μm when GO-to-NS molar ratio is reduced to 5. The specimens with the lowest GO-to-NS molar ratio, 1-GONS-T25 and 1-GONS-T100, are 15.3±0.2 and 23.5±0.5 μm-thick, respectively. It can be noticed that the thickening of X-GONS-TY membranes with respect to pure GO, related to the intercalation of NS moieties within the GO sheets, appears to be consistent with the observations inferred from ATR and Raman spectroscopies.

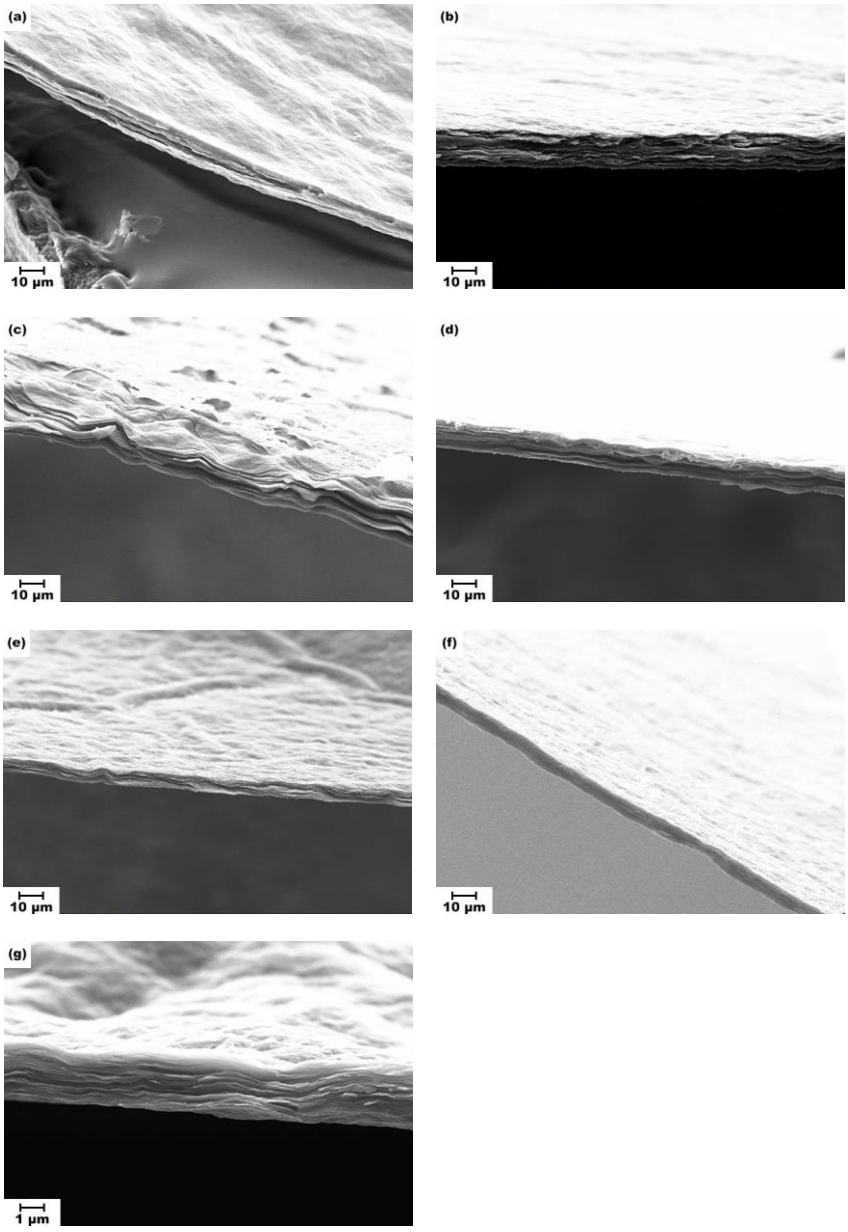

Fig. 7 Cross-sectional SEM images of X-GONS-TY samples at 1000x magnification: (a) 1-GONS-T25, (b) 1-GONS-T100, (c) 5-GONS-T25, (d) 5-GONS-T100, (e) 10-GONS-T25, (f) 10-GONS-T100; (g) GO cross-sectional SEM image at 10000x magnification is reported as reference

Publisher version: https://doi.org/10.1016/j.ssi.2022.115858

Table 2. X-GONS-TY membranes and reference GO thicknesses.

Sample	Thickness [µm]
1-GONS-T25	15.3 ± 0.2
1-GONS-T100	23.5 ± 0.5
5-GONS-T25	17.3 ± 1.1
5-GONS-T100	17.1 ± 0.2
10-GONS-T25	9.7 ± 0.3
10-GONS-T100	7.6 ± 0.2
GO	3.6 ± 0.2

3.2.5 Energy dispersive X-ray spectroscopy

Semi-quantitative elemental analysis of the proposed materials has been performed via energy dispersive X-ray (EDX) spectroscopy to realise the effect of the NS-based sulfonation process on the composition of the products. The extrapolated weight percentages of carbon (C), oxygen (O) and sulphur (S) are shown in Figure 8 and compared with those of a GO reference. The six X-GONS-TY samples exhibit a growth in sulphur content with respect to virgin GO, which is compatible with the hypothesis of an effective combination of NS moieties and GO substrate through the discussed innovative functionalisation protocol. Interestingly, since each sulfonic acid group ($–SO_3H$) bears three oxygen atoms, one would have also expected an increase in the weight percentage of this species, as a consequence of the introduction of naphthalene sulfonates. On the contrary, a visible drop is detected, especially for the T100 samples. The occurrence of a slight reduction of the GO framework which forces the loss of O-bearing moieties, more accentuated when the reaction temperature is higher, can be supposed to elucidate this behaviour. 1-GONS-T100 has the highest sulphur content, coherently with its GO-to-NS molar ratio, but the strong presence of NS molecules has been detrimental in terms of structural stability, inasmuch the membrane has crumbled as soon as it has been recovered from the PVDF filter. 5-GONS-T100 exhibits the second highest sulphur weight percentage and a carbon-to-oxygen ratio (1.495±0.036) close to virgin GO (1.5 [44]), accompanied by an adequate flexibility and manageability.

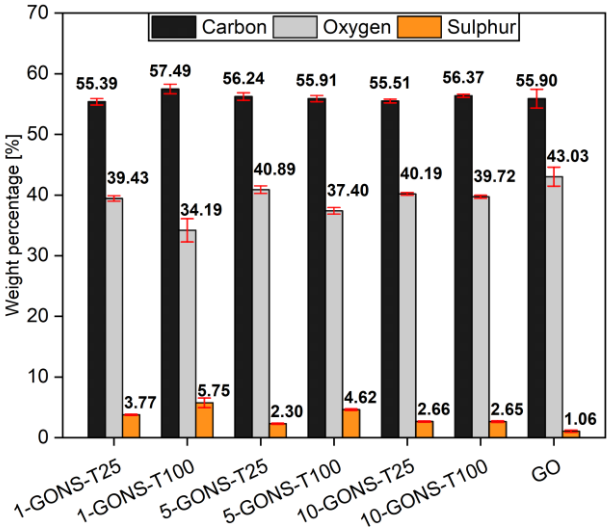

Fig. 8 EDX spectroscopy results of the investigated X-GONS-TY membranes and virgin GO as reference

Publisher version: https://doi.org/10.1016/j.ssi.2022.115858

3.2.6 Optical contact angle

The static optical contact angle evaluation has been executed by means of ten measurements on different positions of each investigated membrane, with the purpose of enhancing the reliability of the results, displayed in Figure 9. The synthesised X-GONS-TY membranes are all included in the hydrophilic interval. 1-GONS-T25 has returned the highest OCA value, surpassing the hydrophilicity limit (dashed horizontal line) when its error interval is considered. This outcome can be explained by the counterbalancing effect of the bulky non-polar naphthenic moieties on the overall water-compatible behaviour of both the oxygenated functionalities in the GO framework and the $–SO_3H$ groups added by the sulfonating agent [57]. The fact that the 10-GONS samples' behaviour is the closest to that of pristine GO (68.98±3.37° [41]) can be taken as a confirmation of this observation, since they possess the lowest NS content. Another possible reason is the slight increase in hydrophobicity induced by the presence of wrinkles on the surface of the specimens [58], as appreciated from SEM images (Figure 6).

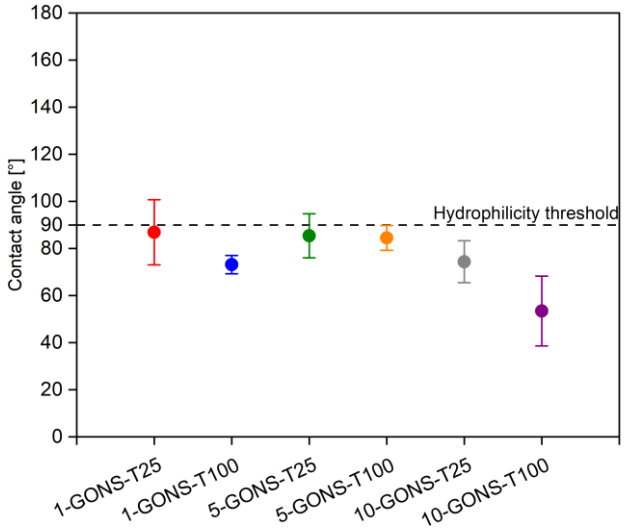

Fig. 9 OCA outcomes of the investigated X-GONS-TY membranes

3.2.7 X-ray diffraction

X-ray diffraction experiments have aimed at checking modifications in the layer spacing of the produced X-GONS-TY membranes and at comparing them to that of pristine GO. The acquired diffractograms allow to observe that GO exhibits an interlayer distance of about 0.82 nm, corresponding to a reflection located at $2\theta = 10.76°$ that describes a 001-reflection plane. This distance is more than twice the intersheet spacing of natural graphite, i.e., 0.34 nm associated to a 002-reflection plane ($2\theta = 26.60°$). The larger interplanar distance of GO may be correlated to the perturbation of the carbonaceous backbone caused by the intercalation of oxygenated functional groups and water molecules amidst of adjacent flakes [26–28,42,59,60].

Concerning X-GONS-TY specimens, their diffraction patterns all exhibit a marked increase in the interlayer spacing with respect to GO, with values in the 0.95–0.88 nm range, corresponding to $2\theta = 9.29–10.05°$. These results may be interpreted as a consequence of the bulky nature of NS molecules and of the corresponding steric hindrance that prevents GO layers to pack more closely and confirms the successful introduction of NS species [32,59].

Publisher version: https://doi.org/10.1016/j.ssi.2022.115858

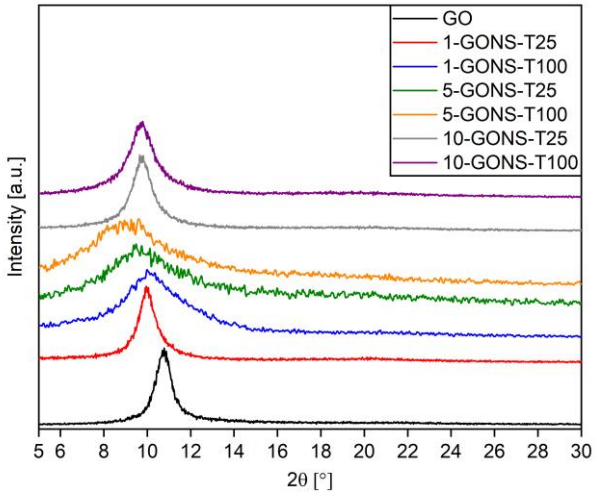

Fig. 10 XRD patterns of the investigated X-GONS-TY membranes

3.3 Ion exchange capacity

Ion exchange capacity (IEC) is a powerful parameter to estimate the quantity of ionic sites that can favour the transport of ions throughout an electrolytic membrane. The outcome of IEC tests carried out on X-GONS-TY specimens is provided in Figure 11.

All average IEC measurements are larger than the one of GO (0.72 meq g^{-1}, determined in a previous work [41]), ranging between a 2-fold and 4-fold improvement. The worst result surprisingly belongs to 1-GONS-T100 (1.46±0.16 meq g^{-1}), which has been prepared with the highest amount of naphthalene sulfonates and has supplied the largest sulphur weight percentage (5.75±0.79 wt.%) via EDX spectroscopy. This information seems quite conflicting, but it can be combined with the increase in the carbon-to-oxygen ratio witnessed in the EDX spectrum to explain the possible occurrence of a moderate partial reduction of the GO skeleton during the studied functionalisation, as suggested in Section 3.2.5. Besides, it must be remembered that EDX is a quite shallow analysis; hence, the high sulphur content measured in 1-GONS-T100 may be caused by an accumulation of unreacted naphthalene sulfonate molecules in-surplus on the surface of the specimen, which do not substantially contribute to the proton exchange mechanism. 10-GONS samples having a better IEC than 1-GONS ones could confirm the detrimental action of an excess of functionalising agent. 5-GONS-T25 and 5-GONS-T100 membranes returned the best IEC determinations, 2.87±0.53 and 2.90±0.03 meq g^{-1} respectively, again recommending that the optimal recipe should be in the neighbourhood of theirs. These values are remarkable, even surpassing the vast majority of the ones achieved by other novel electrolytes illustrated in literature [11,18,28,30]. They recommend a strong tendency to ion exchange phenomena, which is a desired feature in PEMs.

In light of the observations on the rising of bands associated to NS functionalities in ATR-FTIR spectra, the overall best thermal resistance determined by TGA, the best compromise between sulphur content (4.62±0.13 wt.%) and carbon-to-oxygen ratio (1.495±0.036) measured through EDX analysis, an adequate manageability and flexibility, as well as an IEC value of 2.90±0.03 meq g^{-1} with restrained variability, 5-GONS-T100 has proven to be the most promising of the examined innovative X-GONS-TY membranes. Therefore, it has been subjected to water uptake (WU) and electrochemical impedance spectroscopy (EIS) tests, in order to complete its characterisation in terms of evaluation of its water retention ability and proton conductivity in the typical operating conditions of a PEMFC.

Publisher version: https://doi.org/10.1016/j.ssi.2022.115858

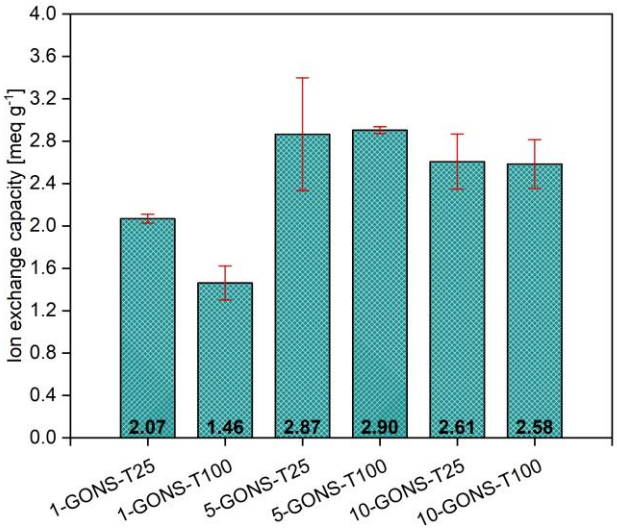

Fig. 11 Ion exchange capacity of the X-GONS-TY membranes

3.4 Water uptake and swelling ratio

Water uptake (WU) and swelling ratio (SR) experimental outcomes of the 5-GONS-T100 membrane are summarised as a function of temperature in Tables 3 and 4.

Table 3. Water uptake and swelling ratio results of 5-GONS-T100 at 53% RH as a function of temperature.

Temperature [°C]	Water uptake [%]	Swelling ratio [%]
20	25.14 ± 1.16	9.84 ± 11.47
40	33.89 ± 2.99	38.17 ± 24.73
60	37.15 ± 5.92	37.61 ± 17.07
80	17.31 ± 1.44	45.82 ± 28.73
100	18.08 ± 9.19	40.31 ± 12.16

Table 4. Water uptake and swelling ratio results of 5-GONS-T100 at 95% RH as a function of temperature.

Temperature [°C]	Water uptake [%]	Swelling ratio [%]
20	20.67 ± 0.72	20.51 ± 8.88
40	24.67 ± 8.00	15.16 ± 9.07
60	30.05 ± 3.05	25.67 ± 20.97
80	45.50 ± 26.80	47.55 ± 26.74
100	18.31 ± 5.00	63.12 ± 4.41

The investigated material exhibits a remarkable water sorption capability at low temperatures and at 53% RH, with a maximum of 37.15±5.92% at 60 °C. In this range, it outperforms both Nafion® 212 and virgin GO, whose detailed analysis has been executed in a previous work amongst the authors' research group [41], presumably due to the hydrophilicity of S-bearing functionalities that allows a considerable permeation and inter-layer trapping of water molecules. At 80 °C, water uptake suffers a significant decrease, but it remains 1.5-fold higher than Nafion®'s (11.34% [41]). Differently, 5-GONS-T100 demonstrates a worse performance than pure GO (32.21% [41]) at the harshest operating conditions, as well as a higher swelling ratio (40.31±12.16%). This last feature may be explained by the proneness to structural weakening

of the GO stacking provoked by the insertion of the sterically bulky naphthenic groups, corroborated by the slight fragility of the specimens; in addition, the highest temperatures may be responsible for a partial removal of the weakest oxygenated moieties and a consequent rise in the hydrophobicity of GO flakes, resulting in weaker attractive interactions and larger swelling. Since SR is considered as a useful parameter to appraise the tendency of the sample to swell when water is adsorbed, a higher value would represent a plausible and undesired failure of the component when sealed in the fuel cell assembly. As a consequence, the structural stability of the material must be enhanced in the view of an application in low humidification PEMFC devices, though the introduction of naphthalene-based molecules has not excessively worsened the properties of the GO substrate.

At 95% RH, the proposed membrane proves again a growing water sorption trend with temperature up to 80 °C, before undergoing a sharp reduction at 100 °C. In detail, outcomes vary from 20.67±0.72% at 20 °C to 30.05±3.05% at 60 °C, overtaking the corresponding ones of Nafion® 212 (from 11.38% to 10.62% [41]) but resulting lower than those of bare GO (from 60.00% to 67.42% [41]). This behaviour suggests a slightly accentuated hydrophobicity of the sample compared to pristine GO (OCA 68.98±3.37° [41]), to be ascribed to the introduction of bulky non-polar naphthenic moieties. Conversely, it can be noticed that 5-GONS-T100's water uptake raises to 45.50±26.80% at 80 °C, whereas its swelling ratio is 47.55±26.74%. The insertion of hydrophilic $–SO_3H$ groups might be able both to positively affect a deeper intercalation of water molecules amidst the GO sheets [34,61] and to partially attenuate the probable GO thermal reduction above 50 °C [41,55] via their higher thermal stability, guaranteeing an adequate behaviour in the examined conditions.

3.5 Proton conductivity

Proton conductivity assessment has relied upon the fitting of the Nyquist plots derived from the electrochemical impedance spectroscopy (EIS) tests, described in Section 2.5. In detail, a modified Randles cell (Figure 12) has been chosen to fit the experimental data [62]. The cell consists of an overall ohmic resistance (R_{el}) in series with a RC element, in turn involving a constant phase element (CPE) in parallel with the internal resistance (R_i) [62–64]. R_{el} corresponds to the intercept of the semicircle in the high-frequency portion of the real impedance axis (Z_{Re}) and stands for the ohmic losses taking place in the system. The CPE replaces the ideal capacitor typical of regular Randles cells, so to better describe the roughness and inherent porosity of the electrode/electrolyte interface, which are responsible for depressed Nyquist arcs. In the end, R_i is the semicircle diameter and characterises the material's internal resistance, useful to compute its conductivity (Equation 4).

Publisher version: https://doi.org/10.1016/j.ssi.2022.115858

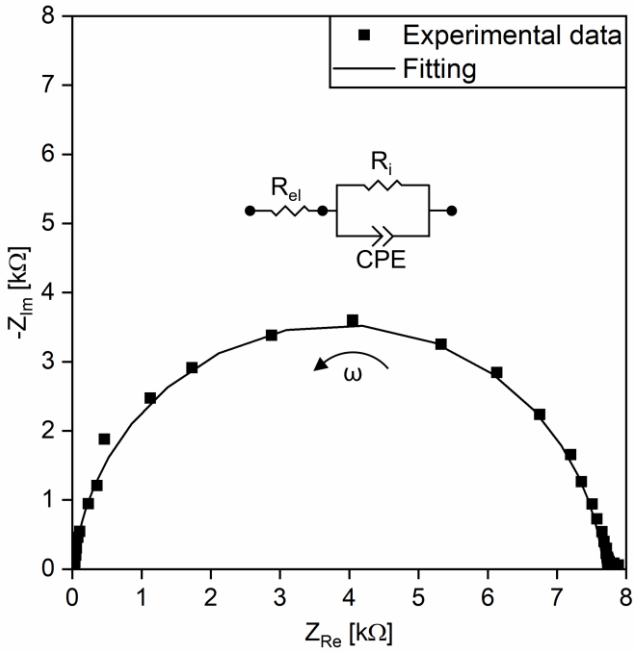

Fig. 12 Measured data (■) and corresponding fitting (—) of 5-GONS-T100, examined at 60 °C, 53% RH. Inset: modified Randles cell, employed for the fitting of the experimental Nyquist plot

Proton conductivity is considered as the fundamental parameter for novel PEMs, since it indicates the suitability of a membrane in fuel cell devices. The average proton conductivities of 5-GONS-T100 are reported in Figure 13 as a function of temperature at 53% and 95% relative humidity (RH). 5-GONS-T100 shows a growing ionic conductivity trend with temperature and relative humidity variations. This behaviour can be linked both to the protons' accelerated mobility due to temperature excitement and to the presence of naphthalene-based structures, which could improve the inter-sheet distribution of $–SO_3H$ functionalities by the generation of π-π interactions between the aromatic portion of the sulfonating agent and the unoxidized zones in the GO structure [34,59]. In this fashion, the risk of a disequilibrium between well-hydrated and dry regions is likely minimised. The role of the introduced $–SO_3H$ groups in 5-GONS-T100 is to amass water clusters via hydrogen bonding, guaranteeing the formation of an efficient proton transport network [65,66]. The correct hydration of the membrane is of paramount importance to enable the transport mechanism known as Grotthuss hopping, which is based on multiple jumps of H^+ ions from a hydrolysed site to the adjacent one within the water molecules network.

At 53% RH, 5-GONS-T100's proton conductivity goes from 0.0354±0.0001 S cm^{-1} at 20 °C to a maximum of 0.2958±0.0312 S cm^{-1} at 80 °C, outperforming bare GO (0.0549±0.0002 S cm^{-1} [41]). This experimental observation confirms that a proper functionalisation of GO is necessary to increase its potentiality as an alternative to Nafion®. The same consideration can be made looking at the 95% RH results attained at 20 and 60 °C. Then, the measured conductivity raises to 1.7135±0.0600 S cm^{-1} at 80 °C, that is roughly one order of magnitude higher than the values reported in literature for the perfluorinated electrolyte [26,42,67]. This outcome is in agreement with the largest WU result monitored in the same conditions and with the abundance of ion exchange sites surveyed through IEC (Section 3.3). It could be ascribed to the microphase separation of hydrophilic and hydrophobic domains favoured by naphthenic moieties and fostering the formation of proton transfer highways. Once more, the effectiveness of the proposed innovative sulfonation protocol is advised, though it must be considered the possibility of a slight distortion of the attained results, ascribable to the employed experimental setup and to the significant presence of condensed water vapour on the electrodes, always detected at the end of the tests.

Publisher version: https://doi.org/10.1016/j.ssi.2022.115858

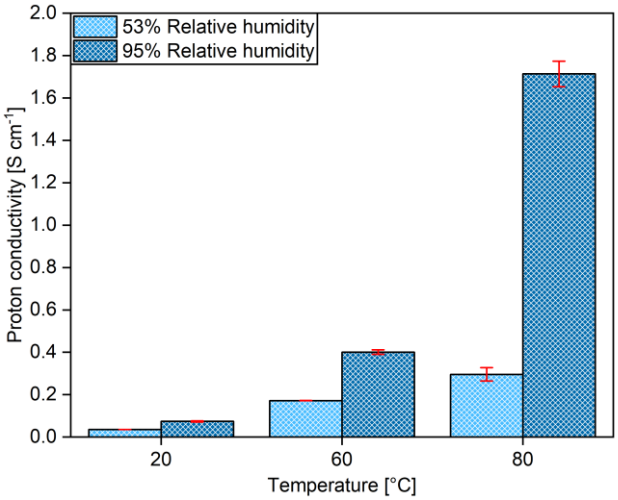

Fig. 13 Proton conductivity of 5-GONS-T100 as a function of temperature at 53% and 95% RH

3.6 Mechanical properties

Tensile strength tests have been executed to verify the mechanical performances of the promising 5-GONS-T100 membrane, in order to acquire information related to its handling, which would be critical during the membrane electrode assembly (MEA) preparation. Moreover, 5-GONS-T100 has undergone micro-hardness indentation tests aimed at evaluating its Vickers hardness. This parameter could be useful to comprehend the membrane surface resistance to compression [68–71], a typical condition to which an electrolyte is subjected in actual fuel cell applications.

Stress-strain curves of 5-GONS-T100 and of reference GO are highlighted in Figure 14, whereas the derived results for tensile strength, elongation at break and Young's modulus are tabulated in Table 5 along with average Vickers hardness values from micro-hardness tests. The mechanical tests conducted on pristine specimens (Figure 14a-b) show that 5-GONS-T100 is extremely stiff with a maximum elongation of 0.18±0.04%, one order of magnitude lower than the one of pristine GO (2.04±0.51%). In the same way, GO's tensile strength (457.9±120.9 MPa) is about one order of magnitude higher than that of 5-GONS-T100 (67.1±7.7 MPa). However, the slope of the curves and, therefore, the Young's moduli of the two materials are comparable. These results implicate that the introduction of NS functionalities does not seem to influence the elasticity of GO layers, but to cause an overall undesired embrittlement of the final product. The restrained variability of the outcomes obtained for 5-GONS-T100 with respect to the ones of virgin GO suggests an enhanced homogeneity of the membrane's structure; this could be potentially associated to the reliability of the 5-GONS-T100 preparation method, resulting in a more uniform stacking of the material's flakes. As shown in Figure 14c-d, both GO and 5-GONS-T100 membranes seem to exhibit an embrittlement after being treated at 80 °C for one hour. This result can be a consequence of a partial removal of oxygenated functionalities taking place at high temperatures, as witnessed from EDX spectroscopy results. However, the previous effect seems to be much more pronounced in GO, while the mechanical behaviour of 80 °C-treated 5-GONS-T100 membranes is fairly consistent with the one of pristine samples, even though displaying a larger variability.

Furthermore, Vickers hardness values recorded for 5-GONS-T100 are moderately higher than the ones of pure GO, both for pristine (20.34±1.06 vs 12.80±0.94 HV) and 80 °C-heated specimens (23.20±3.11 vs 13.27±2.25 HV); these results seem to confirm a slight embrittlement of both GO and 5-GONS-T100 membranes after they are treated at higher temperatures. Considering that hardness and compressive strength are quasi-linearly related [69,70] up to 15% of elongation [68], these results can be exploited to deduce information about the better overall compressive behaviour of 5-GONS-T100. This hypothesis may be reinforced by the immediate failure of GO samples when the load applied during

hardness tests has been raised to 1000 gf, while 5-GONS-T100 has provided comparable performances. This feature can be considered valuable with a view of a potential application in fuel cells, since compressive stresses are among those typical of the closure procedure of a unit assembly.

Table 6 reports a comparison of the ion exchange capacity, proton conductivity and tensile strength performances of 5-GONS-T100 with state-of-the-art PEMs discussed in recent studies. The potentiality of the proposed 5-GONS-T100 blend for fuel cell applications is again suggested by the largest IEC value, second highest proton conductivity and a tensile strength consistent with other innovative materials.

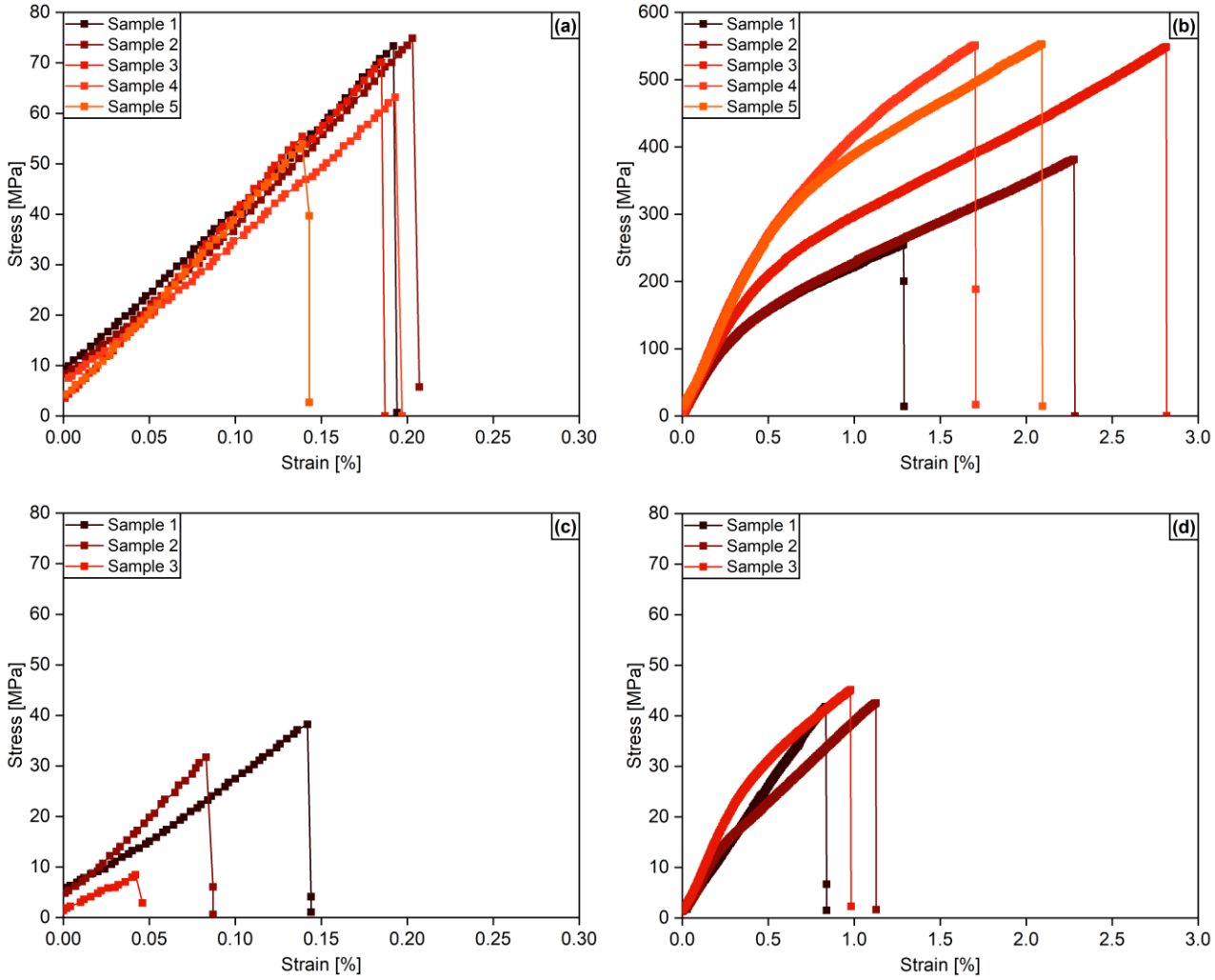

Fig. 14 Stress-strain curves of pristine (a) 5-GONS-T100, (b) GO, and of 80 °C-treated (c) 5-GONS-T100, (d) GO

Table 5. Tensile strength, strain at break, Young's modulus and Vickers hardness results extrapolated from mechanical tests.

Sample	Temperature [°C]	Tensile strength [MPa]	Strain at break [%]	Young's modulus [GPa]	Vickers hardness [HV]
5-GONS-T100	25	67.10 ± 7.70	0.18 ± 0.04	37.41 ± 2.58	20.34 ± 1.06
	80	26.13 ± 15.66	0.08 ± 0.07	21.39 ± 7.50	23.20 ± 3.11
GO	25	457.9 ± 120.9	2.04 ± 0.51	52.92 ± 6.42	12.80 ± 0.94
	80	43.15 ± 1.77	0.98 ± 0.14	5.68 ± 0.63	13.27 ± 2.25

Table 6. Summary of properties and comparison of state-of-the-art PEMs.

Membrane	IEC [meq g^{-1}]	Proton conductivity [S cm^{-1}]	Tensile strength [MPa]	Reference
S-bg-PI/S-r-PI 80:20	1.80	0.30	123.0	[15]
sPSU	1.36	0.0053	15.4	[17]
SPEEK/rGONR@TiO_2	1.63	1.78	64.5	[18]
0.5%v/v S-GO/S-PEKES	0.99	0.0059	45.8	[28]
$(PU/GO/PDDA/GO)_{200}$/85%PA	—	0.391	0.4	[37]
SPVDF$(CS/GO)_{50}$/PA	—	0.234	28.8	[38]
GO	0.72	0.196	457.9	[41], Present work
SGO-1	1.20	0.242	—	[41]
$(PVC/SGO)_5$/85%PA	—	0.0363	19.3	[50]
SFBCN/SPVdF-HFP-10/$FSiO_2$-10	1.61	0.0931	—	[56]
SP/SGO-08	1.45	0.0089	36.5	[65]
PVdF/SPEEK-sCMK-3	1.76	0.081	826.2	[66]
5-GONS-T100	2.90	1.71	67.1	Present work

4. Conclusions

The herein disclosed experimental work has illustrated an effective and simple procedure for the fabrication of naphthalene sulfonate-functionalised graphene oxide (X-GONS-TY) freestanding membranes and a preliminary assessment of their feasibility as innovative electrolytes in proton exchange membrane fuel cells (PEMFCs).

Three different GO-to-NS molar ratios and two different reaction temperatures have been combined to produce six samples, whose extensive analysis has allowed to clarify the effects of the above-mentioned parameters on the properties of the final membranes. Morphological characterisations such as attenuated total reflection Fourier-transform infrared (ATR-FTIR) spectroscopy and thermogravimetric analysis (TGA) have assisted in the evaluation of the sulfonation treatment's effectiveness. In parallel, semi-quantitative EDX elemental analysis has highlighted a simultaneous partial reduction of the GO framework, which can be probably attributed to a thermally induced degradation, obviously more pronounced at higher temperatures. IEC evaluation has helped in defining the abundance of ion exchange sites of each sample, which is fundamental to guarantee an appropriate proton conductivity. Specifically, it has been noticed that the membranes having the highest naphthalene sulfonate content (1-to-1 GO-to-NS molar ratio) display the lowest IEC values, despite they have demonstrated a significant increase in sulphur's weight percentage. This outcome has evidenced the detrimental effect of the intercalation of an excessive amount of NS species, already supposed after the severe fragmentation of the specimen synthesised at 100 °C (1-GONS-T100) when separated from the PVDF filter. Besides, 5-GONS-T100 has yielded the best IEC of 2.90±0.03 meq g^{-1}, suggesting that the optimal molar ratio must be searched in the proximity of 5-to-1. Since it has also shown the best thermal stability and a suitable increase in sulphur's content, it has been identified as the most promising membrane and subjected to water uptake (WU) and electrochemical impedance spectroscopy (EIS) tests at various temperature and humidification conditions. The selected sample has exhibited the best water retention capability and the highest proton conductivity of 1.713±0.060 S cm^{-1} at 80 °C and 95% relative humidity, whereas it has returned the overall highest WU values and a conductivity generally approaching the one of Nafion® at 53% relative humidity. Eventually, the characterisation of 5-GONS-T100 has been completed by means of both tensile

strength and micro-hardness tests. The obtained results have highlighted the fragility of the fabricated membrane, whose elongation at break does not overcome 0.2%, confirming some criticalities in terms of integrity arisen during the manufacturing of larger samples. However, while the resistance to tensile stresses resulted to be poor, the higher Vickers hardness recorded for 5-GONS-T100 with respect to pure GO may suggest a better resistance to compressive stresses typical of a fuel cell assembly, a feature that can be considered valuable. Nevertheless, a fuel cell test has been impossible, inasmuch the membrane could have failed during the MEA fabrication or during the experiment execution, as a consequence of the witnessed brittle behaviour. Further analyses will be fundamental for the validation of the obtained data and for the development of suitable synthesis routes, with the purpose to optimise the functionalisation and to enhance the structural properties of the prepared material. Different GO-to-NS molar ratios in the neighbourhood of 5-to-1 should be investigated to isolate the optimal recipe that permits to manufacture a membrane with a balance between functional and mechanical features. The incorporation of suitable cross-linking agents could also be helpful, so as to reach a sufficient stability that guarantees reliability in the operational environment of a PEMFC.

Funding

This research did not receive any specific grant from funding agencies in the public, commercial, or not-for-profit sectors.

Acknowledgments

The authors would like to express their gratitude to: the Organic Functional and Nanostructured Materials (FuNMat) laboratory of the Department of Chemistry, Materials and Chemical Engineering “Giulio Natta” at Politecnico di Milano, especially in the person of Dr. Luigi Brambilla, whose expertise has been truly helpful to acquire and interpret infrared and Raman spectra; Lorenzo Giudici and the Material Testing laboratory of the Department of Mechanical Engineering of Politecnico di Milano for their crucial support in the execution of mechanical tests.

References

[1] IEA, World Energy Outlook 2019, Paris (FR), 2019. https://www.iea.org/reports/world-energy-outlook-2019.

[2] United Nations, World Economic Situation and Prospects 2020, United Nations publication, New York, NY (US), 2020. https://www.un.org/development/desa/dpad/wp-content/uploads/sites/45/WESP2020_FullReport.pdf.

[3] United Nations - Department of Economic and Social Affairs (Population Division), World Population Prospects 2019: Highlights, United Nations, New York, NY (US), 2019. https://population.un.org/wpp/Publications/Files/WPP2019_Highlights.pdf.

[4] U.S. Department of Energy, DOE Technical Targets for Polymer Electrolyte Membrane Fuel Cell Components, (2020). https://www.energy.gov/eere/fuelcells/doe-technical-targets-polymer-electrolyte-membrane-fuel-cell-components.

[5] S. Latorrata, P.G. Stampino, E. Amici, R. Pelosato, C. Cristiani, G. Dotelli, Effect of rheology controller agent addition to Micro-Porous Layers on PEMFC performances, in: Solid State Ionics, Elsevier, 2012: pp. 73–77. https://doi.org/10.1016/j.ssi.2012.03.030.

[6] S. Satyapal, Hydrogen and Fuel Cells Enabled through the U.S. Department of Energy, ECS Meet. Abstr. (2019). https://doi.org/10.1149/MA2019-01/34/1791.

[7] A.L. Dicks, D.A.J. Rand, Proton-exchange membrane fuel cells, in: Fuel Cell Syst. Explain., 3rd ed., John

Wiley & Sons, Ltd, Chichester (UK), 2018: pp. 69–133. https://doi.org/10.1002/9781118706992.ch4.

[8] T. Bayer, S.R. Bishop, M. Nishihara, K. Sasaki, S.M. Lyth, Characterization of a graphene oxide membrane fuel cell, J. Power Sources. 272 (2014) 239–247. https://doi.org/10.1016/j.jpowsour.2014.08.071.

[9] R. Kumar, K. Scott, Freestanding sulfonated graphene oxide paper: a new polymer electrolyte for polymer electrolyte fuel cells, Chem. Commun. 48 (2012) 5584–5586. https://doi.org/10.1039/c2cc31771k.

[10] X. Sun, S.C. Simonsen, T. Norby, A. Chatzitakis, Composite membranes for high temperature PEM fuel cells and electrolysers: a critical review, Membranes (Basel). 9 (2019) 83. https://doi.org/10.3390/membranes9070083.

[11] B. Wang, Z. Cai, N. Zhang, B. Zhang, D. Qi, C. Zhao, H. Na, Fully aromatic naphthalene-based sulfonated poly(arylene ether ketone)s with flexible sulfoalkyl groups as polymer electrolyte membranes, RSC Adv. 5 (2015) 536–544. https://doi.org/10.1039/C4RA12651C.

[12] K. Pourzare, Y. Mansourpanah, S. Farhadi, M.M. Hasani Sadrabadi, I. Frost, M. Ulbricht, Improving the efficiency of Nafion-based proton exchange membranes embedded with magnetically aligned silica-coated Co3O4 nanoparticles, Solid State Ionics. 351 (2020) 115343. https://doi.org/10.1016/J.SSI.2020.115343.

[13] H. Zhu, M. Jia, Q. Li, C. Zhang, P. Zheng, Research the effect of crosslinking degree on the overall performance of novel proton exchange membranes, Solid State Ionics. 351 (2020) 115325. https://doi.org/10.1016/J.SSI.2020.115325.

[14] N. Esmaeili, E.M. Gray, C.J. Webb, Non-Fluorinated Polymer Composite Proton Exchange Membranes for Fuel Cell Applications-A Review, ChemPhysChem. 20 (2019) cphc.201900191. https://doi.org/10.1002/cphc.201900191.

[15] G. Ito, M. Tanaka, H. Kawakami, Sulfonated polyimide nanofiber framework: Evaluation of intrinsic proton conductivity and application to composite membranes for fuel cells, Solid State Ionics. 317 (2018) 244–255. https://doi.org/10.1016/j.ssi.2018.01.029.

[16] M.A. Haque, A.B. Sulong, E.H. Majlan, K.S. Loh, T. Husaini, R. Rosli, Physiochemical Characteristics of Solid Electrolyte Membranes for High-Temperature PEM Fuel Cell, Int. J. Electrochem. Sci. 14 (2019) 371–386. https://doi.org/10.20964/2019.01.26.

[17] C. Simari, E. Lufrano, G.A. Corrente, I. Nicotera, Anisotropic behavior of mechanically extruded sulfonated polysulfone: Implications for proton exchange membrane fuel cell applications, Solid State Ionics. 362 (2021) 115581. https://doi.org/10.1016/J.SSI.2021.115581.

[18] T. Roy, S.K. Wanchoo, K. Pal, Novel sulfonated poly (ether ether ketone)/rGONR@TiO2 nanohybrid membrane for proton exchange membrane fuel cells, Solid State Ionics. 349 (2020) 115296. https://doi.org/10.1016/J.SSI.2020.115296.

[19] F. Barbir, Main cell components, material properties, and processes, in: PEM Fuel Cells, 2nd ed., Academic Press, Amsterdam (NL), 2013: pp. 73–117. https://doi.org/10.1016/B978-0-12-387710-9.00004-7.

[20] G. Chen, S. Zhai, Y. Zhai, K. Zhang, Q. Yue, L. Wang, J. Zhao, H. Wang, J. Liu, J. Jia, Preparation of sulfonic-functionalized graphene oxide as ion-exchange material and its application into electrochemiluminescence analysis, Biosens. Bioelectron. 26 (2011) 3136–3141. https://doi.org/10.1016/j.bios.2010.12.015.

[21] D.R. Dreyer, S. Park, C.W. Bielawski, R.S. Ruoff, The chemistry of graphene oxide, Chem. Soc. Rev. 39 (2010) 228–240. https://doi.org/https://doi.org/10.1039/B917103G.

[22] M.I. Fadlalla, P.S. Kumar, V. Selvam, S.G. Babu, Emerging energy and environmental application of graphene and their composites: a review, J. Mater. Sci. 55 (2020) 7156–7183. https://doi.org/10.1007/s10853-020-04474-

0.

[23] L. Yang, B. Tang, P. Wu, Metal–organic framework–graphene oxide composites: a facile method to highly improve the proton conductivity of PEMs operated under low humidity, J. Mater. Chem. A. 3 (2015) 15838–15842. https://doi.org/10.1039/C5TA03507D.

[24] K. Pourzare, Y. Mansourpanah, S. Farhadi, Advanced nanocomposite membranes for fuel cell applications: a comprehensive review, Biofuel Res. J. 3 (2016) 496–513. https://doi.org/10.18331/BRJ2016.3.4.4.

[25] O. Vryonis, T. Andritsch, A.S. Vaughan, P.L. Lewin, An alternative synthesis route to graphene oxide: influence of surface chemistry on charge transport in epoxy-based composites, J. Mater. Sci. 54 (2019) 8302–8318. https://doi.org/10.1007/s10853-019-03477-w.

[26] H.C. Chien, L.D. Tsai, C.P. Huang, C.Y. Kang, J.N. Lin, F.C. Chang, Sulfonated graphene oxide/Nafion composite membranes for high-performance direct methanol fuel cells, Int. J. Hydrogen Energy. 38 (2013) 13792–13801. https://doi.org/10.1016/j.ijhydene.2013.08.036.

[27] M. Vinothkannan, R. Kannan, A.R. Kim, G.G. Kumar, K.S. Nahm, D.J. Yoo, Facile enhancement in proton conductivity of sulfonated poly (ether ether ketone) using functionalized graphene oxide - Synthesis, characterization, and application towards proton exchange membrane fuel cells, Colloid Polym. Sci. 294 (2016) 1197–1207. https://doi.org/10.1007/s00396-016-3877-8.

[28] S. Changkhamchom, A. Sirivat, Sulfonated (graphene oxide/poly(ether ketone ether sulfone) (S-GO/S-PEKES) composite proton exchange membrane with high proton conductivity for direct methanol fuel cell, Polym. Technol. Mater. 58 (2019) 1900–1913. https://doi.org/10.1080/25740881.2019.1587770.

[29] K. Feng, B. Tang, P. Wu, Sulfonated graphene oxide-silica for highly selective Nafion-based proton exchange membranes, J. Mater. Chem. A. 2 (2014) 16083–16092. https://doi.org/10.1039/c4ta03207a.

[30] R. Sandström, A. Annamalai, N. Boulanger, J. Ekspong, A. Talyzin, I. Mühlbacher, T. Wågberg, Evaluation of fluorine and sulfonic acid co-functionalized graphene oxide membranes under hydrogen proton exchange membrane fuel cell conditions, Sustain. Energy Fuels. 3 (2019) 1790–1798. https://doi.org/10.1039/C9SE00126C.

[31] C. Redín, F.T. Lange, H.-J. Brauch, S.H. Eberle, Synthesis of Sulfonated Naphthalene-Formaldehyde Condensates and their Trace-analytical Determination in Wastewater and River Water, Acta Hydrochim. Hydrobiol. 27 (1999) 136–143. https://doi.org/10.1002/(SICI)1521-401X(199905)27:3<136::AID-AHEH136>3.3.CO;2-T.

[32] V. Toson, M. Milanesio, E. Conterosito, Crystal packing and layered morphology relationships in naphthalene sulfonate compounds, Zeitschrift Fur Krist. - Cryst. Mater. 232 (2017) 463–469. https://doi.org/10.1515/zkri-2016-2010.

[33] G. Booth, Naphthalene Derivatives, in: Ullmann's Encycl. Ind. Chem., Wiley-VCH Verlag GmbH & Co. KGaA, Weinheim, Germany, 2000. https://doi.org/10.1002/14356007.a17_009.

[34] Y. Shudo, M.R. Karim, R. Ohtani, M. Nakamura, S. Hayami, Hybrids from the π–π Stacking of Graphene Oxide and Aromatic Sulfonic Compounds for Improved Proton Conductivity, ChemElectroChem. 5 (2018) 238–241. https://doi.org/10.1002/celc.201701026.

[35] J.P. Turley, F. Romer, M.L. Trudeau, M.L. Dias, M.E. Smith, J. V. Hanna, D.M. Antonelli, Variable temperature proton conductivity of mesoporous titanium oxides doped with naphthalene sulfonate formaldehyde resin, Microporous Mesoporous Mater. 190 (2014) 284–291. https://doi.org/10.1016/j.micromeso.2014.02.022.

[36] J.P. Turley, F. Romer, M.L. Trudeau, M.L. Dias, M.E. Smith, J. V. Hanna, D.M. Antonelli, Proton conductivity of naphthalene sulfonate formaldehyde resin-doped mesoporous niobium and tantalum oxide composites, ChemSusChem. 8 (2015) 301–309. https://doi.org/10.1002/cssc.201402546.

[37] T. Jia, S. Shen, L. Xiao, J. Jin, J. Zhao, Q. Che, Constructing multilayered membranes with layer-by-layer self-assembly technique based on graphene oxide for anhydrous proton exchange membranes, Eur. Polym. J. 122 (2020) 109362. https://doi.org/10.1016/j.eurpolymj.2019.109362.

[38] S. Shen, T. Jia, J. Jia, N. Wang, D. Song, J. Zhao, J. Jin, Q. Che, Constructing anhydrous proton exchange membranes through alternate depositing graphene oxide and chitosan on sulfonated poly(vinylidenefluoride) or sulfonated poly(vinylidene fluoride-co-hexafluoropropylene) membranes, Eur. Polym. J. 142 (2021) 110160. https://doi.org/10.1016/j.eurpolymj.2020.110160.

[39] D.A. Dikin, S. Stankovich, E.J. Zimney, R.D. Piner, G.H.B. Dommett, G. Evmenenko, S.T. Nguyen, R.S. Ruoff, Preparation and characterization of graphene oxide paper, Nature. 448 (2007) 457–460. https://doi.org/10.1038/nature06016.

[40] S. Latorrata, A. Basso Peressut, P. Gallo Stampino, C. Cristiani, G. Dotelli, Preliminary study on the development of sulfonated graphene oxide membranes as potential novel electrolytes for PEM fuel cells, ECS Trans. 86 (2018) 347–356. https://doi.org/10.1149/08613.0347ecst.

[41] A. Basso Peressut, S. Latorrata, P. Gallo Stampino, G. Dotelli, Development of self-assembling sulfonated graphene oxide membranes as a potential proton conductor, Mater. Chem. Phys. 257 (2021) 123768. https://doi.org/10.1016/j.matchemphys.2020.123768.

[42] M. Vinothkannan, A.R. Kim, G. Gnana Kumar, D.J. Yoo, Sulfonated graphene oxide/Nafion composite membranes for high temperature and low humidity proton exchange membrane fuel cells, RSC Adv. 8 (2018) 7494–7508. https://doi.org/10.1039/c7ra12768e.

[43] G. Dotelli, M.C. Gallazzi, C.M. Mari, F. Greppi, E. Montoneri, A. Manuelli, Polyalkylphosphazenes as solid proton conducting electrolytes, J. Mater. Sci. 39 (2004) 6937–6943. https://doi.org/10.1023/B:JMSC.0000047535.62034.60.

[44] Graphenea, Product Datasheet Graphenea Graphene Oxide (GO), (2019). https://cdn.shopify.com/s/files/1/0191/2296/files/Graphenea_GO_4mgmL_Datasheet_201905.pdf?22.

[45] W.S. Hummers, R.E. Offeman, Preparation of graphitic oxide, J. Am. Chem. Soc. 80 (1958) 1339. https://doi.org/10.1021/ja01539a017.

[46] Z. Pei, L. Li, L. Sun, S. Zhang, X. Shan, S. Yang, B. Wen, Adsorption characteristics of 1,2,4-trichlorobenzene, 2,4,6-trichlorophenol, 2-naphthol and naphthalene on graphene and graphene oxide, Carbon N. Y. 51 (2013) 156–163. https://doi.org/10.1016/j.carbon.2012.08.024.

[47] S. Miao, H. Zhang, X. Li, Y. Wu, A morphology and property study of composite membranes based on sulfonated polyarylene ether sulfone and adequately sulfonated graphene oxide, Int. J. Hydrogen Energy. 41 (2016) 331–341. https://doi.org/10.1016/j.ijhydene.2015.10.080.

[48] P.J. Larkin, IR and Raman Spectra–Structure Correlations, in: Infrared Raman Spectrosc., Elsevier, 2018: pp. 85–134. https://doi.org/10.1016/B978-0-12-804162-8.00006-9.

[49] A. Rahmanian, L. Naji, M. Javanbakht, The influence of sulfonation level on the electrochemical characteristics of Pt/rSGO as electrocatalyst for proton exchange membrane fuels cells, Solid State Ionics. 326 (2018) 27–36. https://doi.org/10.1016/j.ssi.2018.09.010.

[50] J. Jin, J. Jia, D. Song, N. Wang, K. Liu, T. Zuo, Q. Che, A facile strategy to construct layered membranes with

high and stable proton conductivity based on sulfonated graphene oxide, Int. J. Energy Res. (2021) 1–13. https://doi.org/10.1002/er.7385.

[51] V. Georgakilas, J.N. Tiwari, K.C. Kemp, J.A. Perman, A.B. Bourlinos, K.S. Kim, R. Zboril, Noncovalent Functionalization of Graphene and Graphene Oxide for Energy Materials, Biosensing, Catalytic, and Biomedical Applications, Chem. Rev. 116 (2016) 5464–5519. https://doi.org/10.1021/acs.chemrev.5b00620.

[52] K.N. Kudin, B. Ozbas, H.C. Schniepp, R.K. Prud'homme, I.A. Aksay, R. Car, Raman Spectra of Graphite Oxide and Functionalized Graphene Sheets, Nano Lett. 8 (2008) 36–41. https://doi.org/10.1021/nl071822y.

[53] E. Aliyev, V. Filiz, M.M. Khan, Y.J. Lee, C. Abetz, V. Abetz, Structural Characterization of Graphene Oxide: Surface Functional Groups and Fractionated Oxidative Debris, Nanomaterials. 9 (2019) 1180. https://doi.org/10.3390/nano9081180.

[54] A.C. Ferrari, J. Robertson, Interpretation of Raman spectra of disordered and amorphous carbon, Phys. Rev. B. 61 (2000) 14095–14107. https://doi.org/10.1103/PhysRevB.61.14095.

[55] S. Eigler, C. Dotzer, A. Hirsch, M. Enzelberger, P. Müller, Formation and decomposition of CO2 intercalated graphene oxide, Chem. Mater. 24 (2012) 1276–1282. https://doi.org/10.1021/cm203223z.

[56] A.R. Kim, J.C. Gabunada, D.J. Yoo, Sulfonated fluorinated block copolymer containing naphthalene unit/sulfonated polyvinylidene-co-hexafluoropropylene/functionalized silicon dioxide ternary composite membrane for low-humidity fuel cell applications, Colloid Polym. Sci. 296 (2018) 1891–1903. https://doi.org/10.1007/s00396-018-4403-y.

[57] C.O. Ania, B. Cabal, J.B. Parra, J.J. Pis, Importance of the Hydrophobic Character of Activated Carbons on the Removal of Naphthalene from the Aqueous Phase, Adsorpt. Sci. Technol. 25 (2007) 155–167. https://doi.org/10.1260/026361707782398164.

[58] E. Bormashenko, Progress in understanding wetting transitions on rough surfaces, Adv. Colloid Interface Sci. 222 (2015) 92–103. https://doi.org/10.1016/j.cis.2014.02.009.

[59] J. Li, H. Wu, L. Cao, X. He, B. Shi, Y. Li, M. Xu, Z. Jiang, Enhanced Proton Conductivity of Sulfonated Polysulfone Membranes under Low Humidity via the Incorporation of Multifunctional Graphene Oxide, ACS Appl. Nano Mater. 2 (2019) 4734–4743. https://doi.org/10.1021/acsanm.9b00446.

[60] J. Chen, B. Yao, C. Li, G. Shi, An improved Hummers method for eco-friendly synthesis of graphene oxide, Carbon N. Y. 64 (2013) 225–229. https://doi.org/10.1016/j.carbon.2013.07.055.

[61] M. Acik, C. Mattevi, C. Gong, G. Lee, K. Cho, M. Chhowalla, Y.J. Chabal, The role of intercalated water in multilayered graphene oxide, ACS Nano. 4 (2010) 5861–5868. https://doi.org/10.1021/nn101844t.

[62] X.-Z. Yuan, C. Song, H. Wang, J. Zhang, Electrical fundamentals, in: Electrochem. Impedance Spectrosc. PEM Fuel Cells, Springer London, London (UK), 2010: pp. 39–93. https://doi.org/10.1007/978-1-84882-846-9_2.

[63] X.-Z. Yuan, C. Song, H. Wang, J. Zhang, Impedance and its corresponding electrochemical processes, in: Electrochem. Impedance Spectrosc. PEM Fuel Cells, Springer London, London (UK), 2010: pp. 95–138. https://doi.org/10.1007/978-1-84882-846-9_3.

[64] X.-Z. Yuan, C. Song, H. Wang, J. Zhang, EIS equivalent circuits, in: Electrochem. Impedance Spectrosc. PEM Fuel Cells, Springer London, London (UK), 2010: pp. 139–192. https://doi.org/10.1007/978-1-84882-846-9_4.

[65] S. Neelakandan, K. Noel Jacob, P. Kanagaraj, R.M. Sabarathinam, A. Muthumeenal, A. Nagendran, Effect of sulfonated graphene oxide on the performance enhancement of acid-base composite membranes for direct methanol fuel cells, RSC Adv. 6 (2016) 51599–51608. https://doi.org/10.1039/c5ra27655a.

[66] A.S. Ramanujam, N.J. Kaleekkal, P.S. Kumar, Preparation and characterization of proton exchange

polyvinylidene fluoride membranes incorporated with sulfonated mesoporous carbon/SPEEK nanocomposite, SN Appl. Sci. 2 (2020) 688. https://doi.org/10.1007/s42452-020-2464-2.

[67] S. Shi, A.Z. Weber, A. Kusoglu, Structure/property relationship of Nafion XL composite membranes, J. Memb. Sci. 516 (2016) 123–134. https://doi.org/10.1016/j.memsci.2016.06.004.

[68] D.S. Dugdale, Vickers hardness and compressive strength, J. Mech. Phys. Solids. 6 (1958) 85–91. https://doi.org/10.1016/0022-5096(58)90017-6.

[69] S.B. Ainbinder, M.G. Laka, Hardness of polymers, Polym. Mech. 2 (1969) 211–217. https://doi.org/10.1007/BF00860285.

[70] K. Kim, F. Milstein, Relation between hardness and compressive strength of polymer concrete, Constr. Build. Mater. 1 (1987) 209–214. https://doi.org/10.1016/0950-0618(87)90033-X.

[71] A. Da Fonte Porto Carreiro, C.A. Dos Santos Cruz, C.E. Vergani, Hardness and compressive strength of indirect composite resins: effects of immersion in distilled water, J. Oral Rehabil. 31 (2004) 1085–1089. https://doi.org/10.1111/j.1365-2842.2004.01147.x.